
Noble Gases in Seawater as Tracers for Physical and Biogeochemical Ocean Processes

Rachel H. R. Stanley and William J. Jenkins

Abstract

Noble gases are biologically and chemically inert, making them excellent tracers for physical processes. There are 5 stable noble gases: He, Ne, Ar, Kr, and Xe, with a range of physicochemical properties; the diffusivities of the noble gases in seawater differ by approximately a factor of 5 and the solubilities of the noble gases in seawater differ by approximately a factor of 10. This broad range in physicochemical characteristics leads to differing response to physical forcing. Thus, measurements of multiple noble gases made concurrently allow quantification of many physical processes. In seawater studies, noble gas measurements have been used to investigate air-sea gas exchange, allowing explicit separation of the bubble component from the diffusive gas exchange component, and to study equilibration during deep water formation. Argon has been used to quantify diapycnal mixing and the heavier noble gases could be useful in such studies as well. Helium, Ne, and Ar have yielded insights on ocean-cryospheric processes such as sea ice formation and basal melting of glaciers. The isotope ^3He has been used extensively in studies of ocean circulation, and also for quantifying ocean-lithospheric interactions. Additionally, noble gases can be combined with biologically active gases, such as O_2 or N_2 , in order to quantify rates of biological production and denitrification.

1 Introduction

Dissolved noble gases are ideal in situ tracers for physical processes in the ocean because they are biologically and chemically inert and thus respond solely to physical forcing. Additionally,

there are five stable noble gases with a range of solubilities and molecular diffusivities in seawater (Fig. 1). The diffusivities in seawater of the noble gases differ by a factor of seven with helium being the most diffusive (Jahne et al. 1987). The solubilities differ by more than an order of magnitude, with xenon being the most soluble (Smith and Kennedy 1983; Wood and Caputi 1966). The solubilities of the heavier noble gases (Ar, Kr, and Xe) have a strong, non-linear dependence on

R. H. R. Stanley (✉) · W. J. Jenkins
Woods Hole Oceanographic Institution, Woods
Hole, MA 02543, USA
e-mail: rstanley@whoi.edu

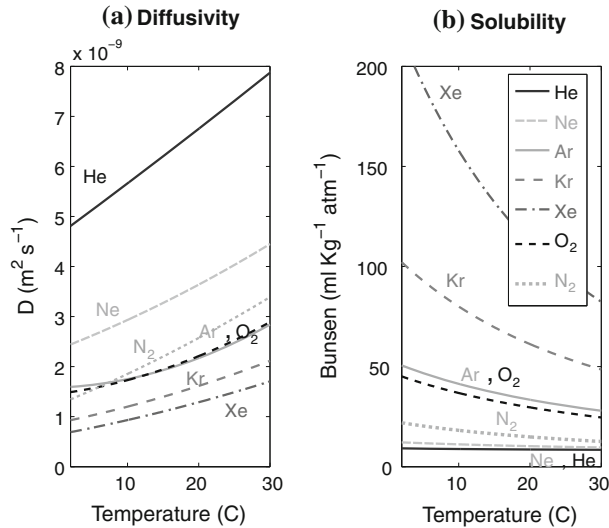


Fig. 1 **a** Molecular diffusivities of the noble gases, oxygen, and nitrogen as a function of temperature, as calculated from the diffusivity values of Jahne et al. (1987) and Wise and Houghton (1966). **b** Solubilities of the five noble gases, nitrogen, and oxygen in seawater as

a function of temperature. Solubility values for He are from a modified version of Weiss (1971), Ne, Ar, and N_2 solubilities are from Hamme and Emerson (2004b), Kr solubility is from Weiss and Kyser (1978) and Xe solubility is from Wood and Caputi (1966)

temperature whereas the solubility of the lighter ones (He, Ne) are relatively insensitive to temperature (Hamme and Emerson 2004b; Smith and Kennedy 1983; Weiss 1971; Weiss and Kyser 1978; Wood and Caputi 1966). Additionally, during sea ice formation or melting, the lighter gases are favorably partitioned into ice whereas the heavier gases remain preferentially in the water (e.g. Hood et al. 1998). This broad range in physicochemical characteristics leads to significantly different responses to physical forcing (Fig. 2). Thus, measurements of multiple noble gases made concurrently in seawater allow one to diagnose and quantify physical processes, such as air-sea gas exchange, diapycnal mixing, and subsurface basal glacial melting.

The main source of noble gases to the ocean is from the atmosphere through the process of air-sea gas exchange. The noble gases are usually close to being in equilibrium with the atmosphere, according to Henry Laws constants, although rapid warming or cooling, ice formation or melting, and bubble injection can lead to departures from

equilibrium. Additionally, He has two additional sources. ^4He is produced by nuclear reactions in rocks, primarily in the Uranium series. Some of this ^4He enters the ocean through water-rock processes. Additionally ^3He is produced by radioactive decay from atmospheric tritium.

Noble gas measurements can be combined with dissolved biologically active gases, such as O_2 or N_2 , to yield quantitative insights into biogeochemical processes. O_2 and N_2 can be used as geochemical tracers for quantifying rates of important biological processes such as net community production and denitrification. However, physical processes such as air-sea gas exchange and thermal forcing affect O_2 and N_2 , making direct interpretation of those gas records difficult. Argon has a very similar solubility and diffusivity to O_2 , and thus can serve as an abiotic analogue to O_2 . Thus, the difference between O_2 and Ar can serve as a tracer for biological productivity. Additionally, Ar can be used in conjunction with nitrogen to construct basin-scale estimates of denitrification.

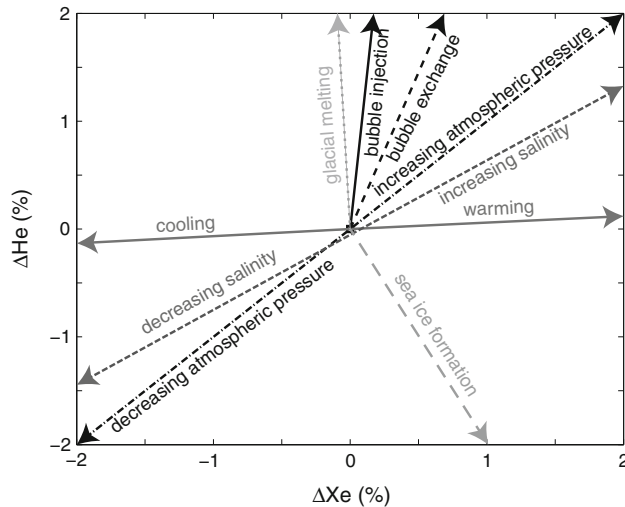


Fig. 2 Schematic depicting the effect of different physical processes on saturation anomalies of He and Xe. Because of the differences in solubilities and diffusivities of the noble

gases, different physical processes have differing effects on the gases, allowing the gases to be powerful tools for separating and quantifying physical processes

2 Analytical Methods

2.1 Sample Collection

The standard protocol for measuring noble gases in seawater is to collect a sample of seawater, extract the gases from the water, and measure the gases on a mass spectrometer. Water samples are generally drawn on the deck of the ship from Niskin bottles mounted on a CTD rosette system. It is important to draw the samples soon after the rosette is retrieved, and immediately after the Niskin is vented for sampling, as exchange with the head-space created from drawing water from the Niskin will compromise the integrity of the dissolved gases (Takahashi et al. 1988). Samples of seawater can be transferred to copper tubes (Weiss 1968; Young and Lupton 1983), stainless steel cylinders (Lott and Jenkins 1998), or pre-evacuated custom-made glass bottles (Emerson et al. 1999) for storage (although the last is not suitable for helium studies). In all cases, great care must be taken when sampling to avoid bubbles entering the sample containers. This can be achieved by presoaking any transfer tubing that is used, tapping on walls of sample containers as the

sample is drawn, keeping the temperature of sample containers similar to temperature of the water (i.e. avoid letting the containers sit in the sun before collecting samples since the gases in the seawater may exsolve due to warming on contact with the container), and carefully watching for any bubbles in tubing, neck of bottle, etc.

The lighter noble gases are more diffusive than the heavier ones and are not well contained by o-rings. If samples are collected in stainless steel cylinders, which have o-rings in the plug valves at the end of the cylinders, it is best to extract the gases from the samples into aluminosilicate glass bulbs within 24–48 h of collection (Lott 2001). If samples are stored in custom-made glass bottles, which contain Louers-Houpert valves that have o-rings, it is best to use valves with two o-rings, to fill the necks with CO₂ to decrease the loss of gas across the valves, and to analyze the samples within at most two months of sample collection (Hamme and Emerson 2004a). In contrast, samples are well preserved in copper tubes for indefinitely long periods.

In the case of stainless steel cylinders, subsequent to sample collection, usually at-sea or in an onshore laboratory, gases are extracted from

the water by essentially boiling the water in a high-vacuum system and transferring the released gas to ~ 25 cc aluminosilicate glass ampoules that can then be flame-sealed and stored. In the laboratory, these ampoules are attached to the mass spectrometer sample processing system using o-ring seals and the sample is introduced by mechanically snapping the end of the glass flame-seal (Lott and Jenkins 1998). In the case of crimped or clamped copper tube samples, a similar extraction procedure can be used on-shore, but after introduction to the evacuated sample line, samples are stirred at room temperature and the aluminosilicate glass ampoules are chilled with liquid nitrogen. Alternatively, some research groups directly attach copper tube samples to the mass spectrometer and extract “in-line” (Beyerle et al. 2000; Sano and Takahata 2005). For the custom-made glass bottles, no extraction is necessary; the gas partitions between the headspace in the bottle and the water (90–99 % in the headspace, depending on the gas) at a known temperature and the water is drained by vacuum filtration prior to analysis (Emerson et al. 1999).

2.2 Sample Analysis

The noble gases are typically analyzed by quadrupole mass spectrometry (QMS) or magnetic sector mass spectrometry. Some methods analyze for only one or two noble gases (Emerson et al. 1999; Hamme and Emerson 2004a) whereas other systems are set up to analyze for all five noble gases from a single sample (Beyerle et al. 2000; Sano and Takahata 2005; Stanley et al. 2009a). The analysis can be conducted by peak height comparison with a standard or by isotope dilution. If the measurements are conducted on an isotope ratio mass spectrometer, then one gas concentration, often Ar, is determined by isotope dilution and the other gases are determined by ratios to that one gas (Hamme and Severinghaus 2007; Severinghaus et al. 2003). The noble gases are commonly chemically purified, often by use of getters, then condensed onto a charcoal and a stainless steel cryogenic trap at 8 K (Stanley et al. 2009a), onto two charcoal traps with one at liquid

N₂ temperature (77 K) and the other at dry ice/acetone temperature (196 K) (Sano and Takahata 2005), or onto a trap at liquid He temperature (4 K) (Hamme and Severinghaus 2007; Severinghaus et al. 2003). Methods that measure all five gases from a single sample have precision of 0.3–1.0 % using a magnetic sector instrument (Beyerle et al. 2000) to 0.1–0.2 % using a series of two automated cryogenic traps and a QMS (Stanley et al. 2009a) and to 0.15–0.17 % for Ar, Kr and Xe only using an isotope ratio mass spectrometer (Hamme and Severinghaus 2007; Severinghaus et al. 2003). Many of the methods also measure a number of different isotopes of each of the noble gases.

When analyzing a sample for a suite of noble gases, one must consider “matrix effects” (also referred to as “chemical slope”) of one noble gas on another, either within the mass spectrometer itself (due to issues such as collisions, competition for ionization, etc.), or within the cryogenic trapping systems used for separating the noble gases. Additionally, the presence of other gases in the instrument such as methane, hydrogen, and nitrogen, have been shown to affect noble gas analysis (Stanley et al. 2009a).

High precision helium isotopic analysis is usually performed on a branch tube magnetic sector mass spectrometer using simultaneous collection of the two isotopes. Helium can be readily separated from other gases by chemical gettering and cryogenic separation (Lott and Jenkins 1984, 1998). Because of the large isotope ratio (${}^4\text{He}/{}^3\text{He} \sim 10^6$) ${}^4\text{He}$ is measured with a faraday cup and electrometer while ${}^3\text{He}$ is measured by pulse counting with an electron multiplier. With a stable system, the ultimate limitation to the precision of the measurement is ${}^3\text{He}$ ion counting statistics. For a “typical” 50–100 g water sample with approximately atmospheric helium isotope ratio, a precision of 0.15 % is commonly achieved.

2.3 Solubilities in Water and Seawater

When exposed to the atmosphere, the noble gases dissolved in seawater will tend to come to

equilibrium concentrations. For each noble gas, these solubility concentrations are a function of temperature, salinity, and pressure. Physical processes such as bubble injection, rapid temperature changes, and ice formation/destruction serve to drive gas concentrations away from solubility equilibrium (Fig. 2), so it is the saturation anomalies (deviations from solubility equilibrium) that are the important observables. Determinations of solubility equilibrium concentrations as a function of temperature and salinity have been made in the laboratory (Hamme and Emerson 2004b; Smith and Kennedy 1983; Weiss 1971; Weiss and Kyser 1978; Wood and Caputi 1966), but with varying degrees of accuracy (e.g. Hamme and Emerson 2004b; Hamme and Severinghaus 2007). The size of noted discrepancies (and hence uncertainties in saturation anomalies) are often significant compared to the effects observed, especially for Xe, and hence limit the quantitative strength of interpretation. It is hoped that the current expansion of interest in oceanic noble gas abundances will motivate a new effort to refine these measurements to at least the quality of the current measurement capability.

3 Air-Sea Gas Exchange

One of the very fruitful applications of noble gases is the determination of air-sea gas exchange fluxes. Air-sea gas exchange is a crucial part of the biogeochemical cycle of climatically important gases (CO₂, DMS, N₂O). Additionally, accurate knowledge of air-sea gas exchange fluxes is imperative when using gases as tracers for biogeochemical processes. Air-sea gas exchange fluxes are very difficult to measure directly and thus most researchers use parameterizations that yield air-sea gas exchange fluxes in terms of easily measured variables such as wind speed. Noble gases are potentially powerful tools for diagnosing air-sea exchange processes, since their distributions are controlled by purely physical and physicochemical mechanisms. Molecular diffusivity, which varies by a factor of seven over the suite of noble gases,

plays an important role both in diffusive air-sea gas exchange and in bubble injection processes. Solubility, and in particular its dependence on temperature, which varies by more than an order of magnitude over the suite of noble gases, is an important driver for gas exchange when significant heat transfer occurs, either during radiative warming in the summer months, or in water mass formation processes during the winter. Thus the contrasting behaviors of noble gases are useful diagnostics of a potentially complex interplay between different processes in the oceanic environment.

3.1 Separating Bubble Component from Diffusive Gas Exchange

Wave action at the sea surface forms bubbles (most visibly in “white caps”) that can be carried downward many meters in the water column by vertical water motions and turbulence (e.g. Thorpe 1984). Increasing hydrostatic pressure with depth tends to force the bubbles to partially or completely dissolve, tending to enhance dissolved gas concentrations. Helium and Ne are the least soluble noble gases and therefore are most sensitive to bubble processes. Argon, Kr and Xe are the most soluble noble gases with a strong temperature dependence to solubility and are thus more sensitive to diffusive gas exchange. Initial work used a time-series of only two noble gases, He and Ar (Spitzer and Jenkins 1989) or Ne, Ar, and N₂ (Hamme and Emerson 2006) to separate diffusive gas exchange from bubble processes. In both studies, bubble processes were further separated into two end-members (Fuchs et al. 1987; Jenkins 1988b): (1) some bubbles, typically small ones, that dissolve completely and therefore inject air of atmospheric abundances and (2) other bubbles, typically larger ones, that are injected, partially dissolve, and then rise back to the surface, therefore fractionating the noble gases according to permeation rate. Hamme and Emerson (2006) found at the Station ALOHA in the subtropical Pacific that bubble flux was important for Ar—and therefore by extension for O₂—and that the ratio of

completely to partially trapped bubble fluxes is between 1:1 and 2:1.

Including all five noble gases (He, Ne, Ar, Kr and Xe) increases the power of noble gases for constraining air-sea gas exchange rates (Stanley et al. 2006; Stanley et al. 2009b), yielding constraints on the diffusive part of gas exchange to $\pm 10\%$ and the bubble component to $\pm 15\%$. A three-year time-series of all five noble gases in the Sargasso Sea (subtropical North Atlantic) illustrates the difference in response of the noble gases to physical forcing (Fig. 3). Helium and Ne are supersaturated by several percent in the upper 150 m and show relatively little seasonal variation, due to a first order balance between bubble injection and diffusive gas exchange. In contrast, Ar, Kr and Xe show a strong seasonal cycle, with large saturation anomalies in the summer, particularly below the mixed layer, produced by seasonal warming. By combining inverse modeling with the noble gas data, Stanley et al. (2009b) produced a parameterization of air-sea gas exchange that explicitly includes bubble processes, is based on an intermediate and relevant time scale, and has tighter constraints than many existing parameterizations. They too found that bubble injection is important for all noble gases, even the more soluble ones such as Xe, and by extension is likely to be important for CO_2 in high wind speed events. Additionally, they found that completely trapped bubbles, i.e. “injected” ones were much more important than partially trapped ones, i.e. “exchanged” ones, with completely trapped bubbles comprising $>90\%$ of the bubble flux in most cases.

Numerical modeling must be combined with the noble gas data in order to constrain air-sea gas exchange. Bulk mixed layer models (PWP), which have been modified for use with the noble gases (Hamme and Emerson 2006; Spitzer and Jenkins 1989; Stanley et al. 2006; Stanley et al. 2009b) are used in the studies mentioned above. Additionally, Ito et al. (2011) have included Ne and Ar into the off-line ECCO model (MIT-GCM) in order to examine gas exchange and diapycnal diffusivity in the Pacific Ocean.

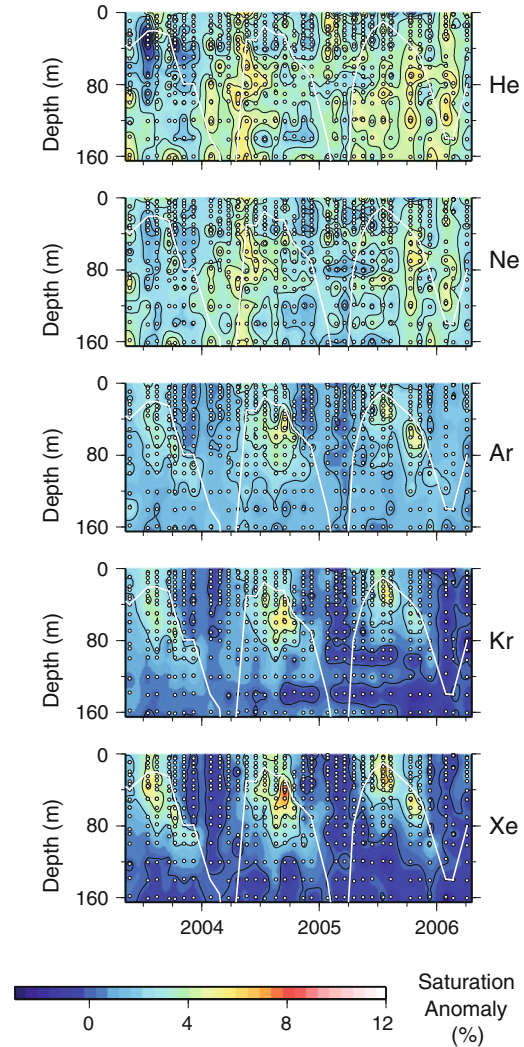


Fig. 3 Saturation anomalies of the five noble gases, calculated from in situ temperature and salinity, in the upper 160 m of the Sargasso Sea, as measured in a three year time-series at the Bermuda Atlantic Time-Series study site. Because the noble gases track physical processes and have a wide range of solubilities and molecular diffusivities, measurements of all five noble gases provide tight constraints on air-sea gas exchange rates. The *white dots* correspond to sample depths and the *thin white line* denotes the mixed layer depth. Figure modified from Stanley et al. (2009b)

Additionally, the noble gas ^3He has been used in conjunction with the gas SF_6 to quantify air-sea gas exchange (Ho et al. 2006, 2011; Nightingale et al. 2000; Salter et al. 2011; Smith et al. 2011; Watson et al. 1991). This approach

yields parameterizations of air-sea gas exchange on time-scales of several days and does not distinguish between bubble-mediated and diffusive gas exchange. The approach rests on the fact that ^3He and SF_6 , both inert gases, have very different gas transfer rates, with ^3He being exchanged quickly and SF_6 being exchanged much more slowly. A known mixture of ^3He and SF_6 is deliberately injected into a patch of water. The patch is followed and the decline in gas concentration is measured over several days; the change in the ratio of the gases is used to quantify air-sea gas exchange. Several parameterizations determined by this dual tracer approach are widely used (Ho et al. 2006; Nightingale et al. 2000).

3.2 High Latitude Ventilation

Air-sea gas exchange processes are important in setting gas concentrations during water mass formation in the high latitudes. Water in the high latitudes is rapidly cooled, leading to an undersaturation of some gases, and there has long been the question of the extent to which gases reach equilibrium before the water is subducted. This question is particularly important for evaluating the strength of the solubility pump of CO_2 . Noble gases can be used to determine the degree to which gases reach equilibrium. Hamme and Severinghaus (2007) used noble and inert gas concentrations (Ne, Ar, Kr, Xe, and N_2) in the intermediate and deep waters at Station ALOHA in the subtropical North Pacific and a time-dependent model of deep convection in the Labrador Sea to examine the relative importance of bubble injection, gas exchange due to cooling, and sea level pressure for setting deep ocean concentrations of gases. The difference in physicochemical properties of the noble gases allowed separation of the processes. Deep water Ne saturation anomalies are positive (i.e. supersaturated) due to the influence of bubbles and the relative insensitivity to rapid cooling (Fig. 4). In contrast, deep water Ar, Kr and Xe saturation anomalies are negative (i.e. undersaturated) due to rapid cooling. It is clear that it is rapid cooling, and not sea level pressure, that causes these undersaturations

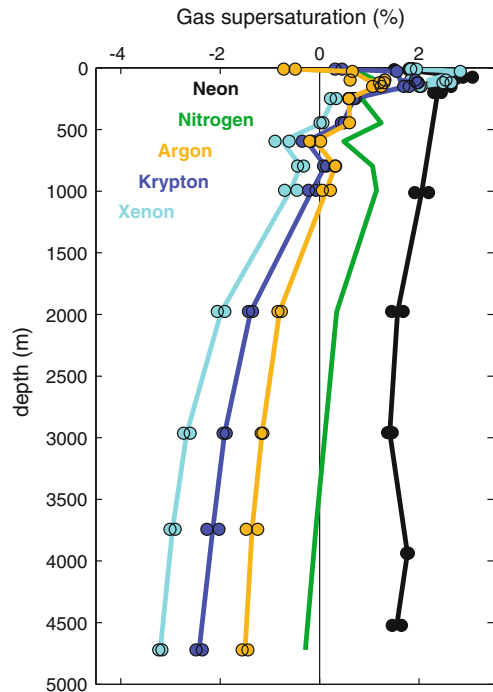


Fig. 4 Depth profiles of Ne, N_2 , Ar, Kr and Xe saturation anomalies measured at station ALOHA in the subtropical North Pacific. Equilibrium with the atmosphere is indicated by the vertical line at 0 %. Points indicate individual samples while the lines are average of duplicates. Xe supersaturations were increased by 2 % above the solubility data of Wood and Caputi (1966). Profiles of deep water noble gas saturation anomalies can constrain the extent to which equilibrium is reached during high latitude ventilation. Figure reproduced from Hamme and Severinghaus (2007)

because sea level pressure variations would affect all gases equally but the undersaturation is stronger for Kr and Xe than for Ar.

Noble gas measurements have also been used in conjunction with three box and seven box models, to examine the extent at which high latitude waters reach equilibrium before ventilation. Nicholson et al. (2010) used profiles of Ar, Kr, as well as Ar isotopes from the northwest Pacific, subtropical North Pacific, and tropical Atlantic oceans to estimate the size of the high latitude ventilation area. They showed that the area for high latitude ventilation is much smaller than the area of enhanced preformed nutrients, suggesting that the CO_2 solubility pump is weaker than box models previously predicted.

4 Diapycnal Mixing

Noble gases are powerful tools for constraining diapycnal mixing rates in the ocean interior. Constraining diapycnal mixing rates is important for understanding the transport of heat and nutrients in the ocean. As Bieri et al. (1966) first suggested, noble gas measurements can be used to estimate basin-scale diapycnal diffusivity coefficients. Models of different complexity, ranging from simple theoretical schematics and box models (Henning et al. 2006; Ito and Deutsch 2006; Ito et al. 2007) to GCMs (Henning et al. 2006; Ito et al. 2011) have been used to show the effects of diapycnal diffusivity on Ar saturation. Including other noble gases in the analysis would likely offer better constraints on diapycnal diffusivity since Kr and Xe have stronger temperature dependence to solubility and a smaller contribution from bubbles.

The basic premise behind this approach is that because of the curvature in the dependence of solubility of the heavier noble gases (Ar, Kr, Xe) on temperature, mixing between water of two different temperatures leads to a positive saturation anomaly (Fig. 5). The magnitude of this saturation anomaly depends on the temperature difference of the waters being mixed. The behavior of noble gases is conservative in the ocean interior. Thus the observed saturation anomaly of a noble gas in the ocean interior can be considered a sum of two components: (1) a preformed component based on gas exchange, bubble injection, and sea level pressure variations when the water was subducted and (2) a mixing component that is the product of noble gas solubility, mixing ratio of low latitude surface waters, and temperature gradients (Ito and Deutsch 2006). Therefore measurements of noble gas saturation anomalies along a transport path from an outcrop to the ocean interior can be used to constrain the diapycnal diffusivity rate. Ito et al. (2007) used Ar data from the North Pacific in order to estimate a diapycnal diffusivity rate of $0.35 \pm 0.21 \times 10^{-4} \text{ m}^2 \text{ s}^{-1}$. However, uncertainties arise from interannual variability in air-sea fluxes at the

outcrop, bubble effects, strong thermal gradients and sparse sampling.

Modeling studies have shown that this method is most promising for the subtropical gyres (Henning et al. 2006; Ito et al. 2011) and indeed the only study actually using data to determine the mixing rates was in the subtropical gyres (Ito et al. 2007). The approach does not work well if the advective time scale is shorter than the diffusive time scale, for example in the equatorial regions, in the strong Western boundary currents (i.e. Kuroshio or Gulf Stream), or in the unventilated shadow zones (Gehrie et al. 2006; Henning et al. 2006; Ito et al. 2011).

5 Ocean-Cryospheric interaction

The interaction of the ocean with the cryosphere, either by seasonal sea ice formation and destruction, or the subsurface melting of grounded glaciers, plays an important role in modifying the density properties of seawater and hence in the formation of deepwater. The presence of a separate phase, namely ice, creates a potential for affecting the dissolved gas composition of seawater. The creation and destruction of sea ice, for example, may serve to differentially enhance or deplete gases according to their respective solubilities in the ice lattice (Fig. 2). The noble gases are potentially unambiguous tools for detecting and quantifying the relative contributions of these processes because of their conservative nature in seawater. We mention three different applications, two of which have been at least partially exploited, and one that may hold promise in the future.

5.1 Sea Ice Formation and Destruction

In polar regions, rapid extraction of heat can form sea ice, a process that increases the density of the remaining seawater by increasing salinity due to brine rejection. This contributes to the formation of deep and bottom waters and potentially to the planetary scale overturning circulation. The formation of ice serves to fractionate gases based on

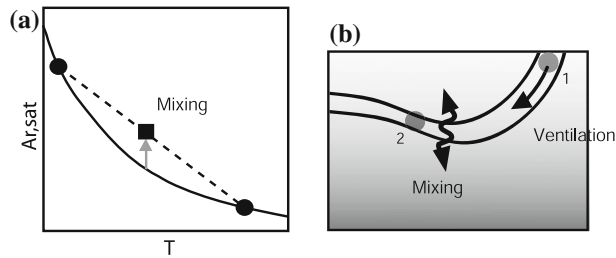


Fig. 5 Cartoons depicting the effect of diapycnal mixing on argon saturation state. **a** Because of the non-linearity of the solubility temperature dependence of Ar (*solid line*, curvature exaggerated for clarity), mixing of two water masses (*filled circles*) produces Ar saturation anomalies above a conservative mixing line (*dash line*). **b** Diapycnal

mixing increases the Ar saturation anomaly whereas horizontal ventilation brings the Ar saturation anomaly toward its surface value. The relative strength of diapycnal mixing vs. horizontal ventilation determines the gradient of the Ar saturation anomaly along an isopycnal surface. Figure reproduced from Ito et al. (2007)

their atomic or molecular size: the ice lattice can accommodate only the smaller species while it rejects the larger ones. This was observed in ice covered stratified Antarctic lakes (Hood et al. 1998) where several fold supersaturation in Ar was observed coincident with a several fold undersaturation of He and Ne. This was argued to be the result of the fact that He and Ne were more soluble in ice than in water, while Ar (and by inference Kr and Xe) were much less soluble in ice than in water.

Laboratory experiments confirmed this differential solubility effect in fresh water and seawater for He, Ne, and Ar (Postlethwaite 2002; Runham 2001) and a time-series in a coastal salt water lagoon on Hokkaido (Postlethwaite 2002) showed similar effects. A subsequent noble gas study in the Japan/East Sea by Postlethwaite et al. (2005), combined with oxygen isotopes, provided some evidence of the contribution of sea ice formation in the Tatarskiy Strait to bottom water formation in that basin.

5.2 Basal Melting of Glaciers

The formation of glacial ice is a complex process that results in the entrapment of air bubbles. Glaciers near the coast often flow toward and into the sea where they extend outward. Contact between relatively warmer seawater and the underside of floating ice shelves results in melting of the ice and release of ice-entrapped bubbles at elevated hydrostatic pressure. This in

turn leads to large observed excesses of He (Schlosser 1986; Schlosser et al. 1990; Weppernig et al. 1996) and likely other noble gases. The injection of these gases has a slightly different signature than the injection of air bubbles from air-sea gas exchange because the melting of the glacial ice also changes the salinity and temperature of the water (Fig. 2). Schlosser and co-workers (Schlosser 1986; Schlosser et al. 1990; Weppernig et al. 1996) pointed to dissolved He excesses in polar waters as resulting from the sea-water induced melting of the ice shelf at high hydrostatic pressure: a signature of the forced dissolution of atmospheric gases occluded in the ice during melting at depth (Gow and Williamson 1975; Martinerie et al. 1992). In combination with other tracer information (particularly stable isotopes) they very effectively used this to constrain the role of sub-glacial melt-water in the formation of Weddell Sea bottom water.

More recently, this approach has been extended into the southeast Pacific to include Ne, and applied to estimate the volume flux of melt-water from the western Antarctic shelves to be of order 7 mSv (Hohmann et al. 2002). A He–Ne simulation based on a regional coupled ice-ocean circulation model has been published (Rodehacke et al. 2007) that reveals not only the diagnostic potential of He and Ne, but also that they not surprisingly serve to “low-pass filter” seasonal/regional variability on the time-scales near the flushing time of the sub-shelf ice

cavern; viz., 2–3 years. He and Ne data, along with the stable isotopic ratio of water ($\text{H}_2^{18}\text{O}/\text{H}_2^{16}\text{O}$), have been used on the Ross Ice Shelf to estimate the concentration of glacial meltwater in that environment (Loose et al. 2009). By combining the meltwater concentration with age estimates calculated by CFC transit time distribution curves, Loose et al. (2009) calculated a basal melting rate for the ice shelf.

One challenge, however, with the interpretation of He and Ne anomalies alone is that air injection associated with air bubbles produced by surface waves and forced into solution hydrostatically can generate saturation anomalies in approximately the same ratio as that inferred from glacial melt: 0.78 vs. 0.76 respectively. Although the authors in the above studies make convincing arguments based on the spatial distribution of the anomalies such that the effects are safely attributed to glacial melting, there still exists the potential for an underlying residual ambiguity. The Ar/Ne and Ar/He ratios of the gases trapped in glacial ice are approximately half the atmospheric ratio (Huber et al. 2006). Therefore, measurement of Ar (and also Kr and Xe) anomalies in seawater offers an opportunity to resolve this ambiguity and obtain a more accurate assessment of glacial melt input.

5.3 Underplating of Floating Ice Shelves

Basal melting of ice shelves produces colder and less saline water at depth that, because it is more buoyant than surrounding seawater, tends to flow upward under the shelf, entraining surrounding waters. This Ice Shelf Water (ISW), as it decompresses, becomes supercooled and forms frazil ice crystals that underplate the shelf (Smedsrud and Jenkins 2004). This process results in accretion of large amounts of submarine ice on the base of the shelf (Holland et al. 2007). The formation of marine ice may result in strong fractionation favoring the larger atomic diameter gases (Ar, Kr, and Xe) relative to He (and possibly Ne) in the residual ISW. In principle,

measurement of the suite of noble gases in ISW emerging from under, for example, the Ronne Ice Shelf could provide valuable constraints on the magnitude of such processes.

6 Ocean Circulation

Tritium (^3H) decays with a 12.31 year half-life (MacMahon 2006) to ^3He , a stable, noble gas isotope. The primary source of ^3H to the contemporary ocean is from ^3H created by the atmospheric thermonuclear bomb tests in the 1960s. Thus, the $^3\text{H}/^3\text{He}$ system is most useful for dating water that has been at the surface within the last 50 years. When the water is at the surface, excess ^3He , i.e. ^3He concentration above the solubility value, is almost completely lost due to gas exchange with the atmosphere. ^3He is measured as the $^3\text{He}/^4\text{He}$ isotope ratio (R) anomaly of the sample (X) relative to the atmospheric standard (A), defined as

$$\delta^3\text{He} = 100 \left(\frac{R_X}{R_A} - 1 \right)$$

When in equilibrium with air, seawater is depleted in ^3He since it is slightly less soluble than ^4He (Benson and Krause 1980; Weiss 1970), with $\delta^3\text{He} \sim -1.7\%$. As water descends from the surface layer and ages, excess ^3He builds up and ^3H correspondingly decreases. The sum of ^3He and ^3H , ζ , acts as a dye-like, stable tracer that responds to mixing and dilution and thus is useful for studying ocean circulation and thermocline ventilation (Jenkins 1987, 1991, 1998). Additionally, ^3He (φ) and ^3H (ϑ) concentrations can be combined with the radioactive decay equation to calculate the tritium- ^3He age, τ , of the water, a measure of time since a water parcel left the surface (Jenkins 1977; Jenkins 1987; Jenkins, et al. 1972) according to

$$\tau = \frac{1}{\lambda} \log \left(1 + \frac{\varphi}{\vartheta} \right)$$

where λ is the radioactive decay constant for ^3H .

Figure 6 depicts the distribution of tritium- ^3He age in years on a constant density anomaly horizon ($\sigma_0 = 26.5 \text{ kg m}^{-3}$) in the Pacific, largely based on World Ocean Circulation Experiment (WOCE) stations taken during the late 1980s and early 1990s. We plot properties on a potential density horizon because the ocean is density stratified and water tends to move along these horizons. This horizon corresponds to the approximate base of the directly ventilated layer in the North Pacific and the main thermocline in the South Pacific (Huang and Qiu 1994, 1998). It lies at a depth of about 200 m in the tropics, deepens to about 500–600 m in the western subtropics, and shoals to the ocean surface in the high latitudes. The distribution of tritium- ^3He ages is a semi-quantitative representation of the ventilation time-scales of this horizon (see discussion below) and bears a general resemblance to other ventilation tracer age distributions such as CFC-ages (Doney et al. 1997; Warner et al. 1996). Note the penetration of younger waters emanating from the high latitude southeast South Pacific and northwest North Pacific, and the fact that the mid-latitude contour lines show an imprint of the large-scale anticyclonic gyre circulation. The age distributions are also characterized by intense, poorly ventilated shadow zones (Luyten et al. 1983) in the eastern equatorial and subequatorial Pacific. These regions coincide with very low tritium values (and hence weak ventilation) and zonally extended, high nutrient plumes that straddle the equator.

It is possible that the tritium- ^3He age distributions shown in Fig. 6 may be influenced by an additional source of non-atmospheric ^3He , namely volcanic ^3He released from sea-floor spreading centers (see Sect. 7). However, despite the relatively large volcanic ^3He plumes evident in Pacific deep water, there are several reasons to suspect that volcanic ^3He does not strongly influence the shallow tritiogenic ^3He distributions in the subtropical and tropical regions. The first stems from the recognition that abyssal waters are more slowly ventilated than the shallow, wind-driven circulation. The deep waters overturn on century-to-millennium time-scales while the

shallow thermocline is ventilated on decadal time-scales. Thus, the abyssal volcanic ^3He plumes are larger due to longer accumulation times.

Second, it is known from hydrography, tracers, and inverse models that the circulation and exchange of shallow and deep waters in the Pacific are not strongly linked (e.g., Wijffels, et al. 1996; Wijffels, et al. 2001), with the bulk of Pacific deep waters (and hence the volcanic ^3He signature) being exported to the Antarctic Circumpolar circulation (Well, et al. 2003). Third, the meridional distribution of excess ^3He in the Pacific is dominated in the vertical by a *minimum* at a potential density anomaly level of approximately $26.8\text{--}27.0 \text{ kg m}^{-3}$ (Jenkins 1996) suggesting little upward transport of volcanic ^3He into the thermocline from below. This can be seen in the meridional distribution of this isotope in the Pacific (along 135°W , Fig. 7). In the upper part of the northern subtropical water column, the ^3He distribution has a characteristic tritiogenic maximum in the thermocline (at about 500 m depth near 30°N) that shoals southward into the tropics. This maximum, also seen in Atlantic waters (see Jenkins 1988b) bears a striking relationship with the observed tritium distribution (see Fig. 8), tracking the tritium plume penetration southward into the tropics. Note the hemispheric asymmetry in the tritium distributions (and the consequent asymmetry in the tritiogenic ^3He) due to the dominant northern hemispheric delivery of this isotope due to the bomb tests (Doney, et al. 1992; Weiss and Roether 1980). A ^3He minimum lies below the tritiogenic ^3He maximum, separating the ventilated (and tritiated) shallow waters from the deeper volcanic ^3He contaminated waters. The depth of this minimum ($\sim 800 \text{ m}$) corresponds to the zero in vertical velocity observed in Wijffels' (2001) inverse calculations.

Finally, one needs to consider the comparative magnitudes of the volcanic and tritiogenic ^3He fluxes. The global volcanic ^3He flux has been estimated to be between 500 and 1,000 mol y^{-1} (Bianchi et al. 2010; Farley et al. 1995), corresponding to an average flux of

Fig. 6 The distribution of tritium- ^3He age (in years) on the 26.5 kg m^{-3} potential density anomaly horizon in the Pacific, as measured during the World Ocean Circulation Experiment (1989–1995). *Grey dots* indicate sampling locations. The depth of this horizon ranges from the near surface in high latitude regions to in excess of 600 m in the western subtropics, and shoals to 100–200 m in the tropics (see map in *upper right* of figure)

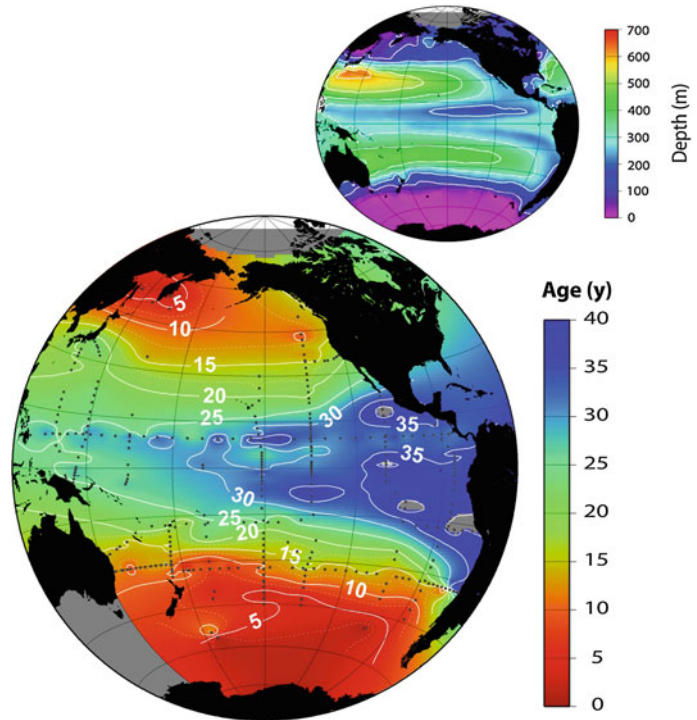


Fig. 7 The distribution of helium isotope ratio anomaly (in percent) plotted as a function of latitude and depth in meters (*upper panel*) and potential density anomaly in kg m^{-3} (*lower panel*) along WOCE line P17(135°W) in 1991. *Black dots* show sample locations. Positive latitude is north, negative is south. The contour (*white lines*) interval is 1 % and measurement precision is 0.15 % (1 sigma). The *grey area* in the *top part* of the *lower panel* corresponds to density anomalies lighter than the shallowest waters for the corresponding locations. Station locations are indicated as a *red line* in the insert map

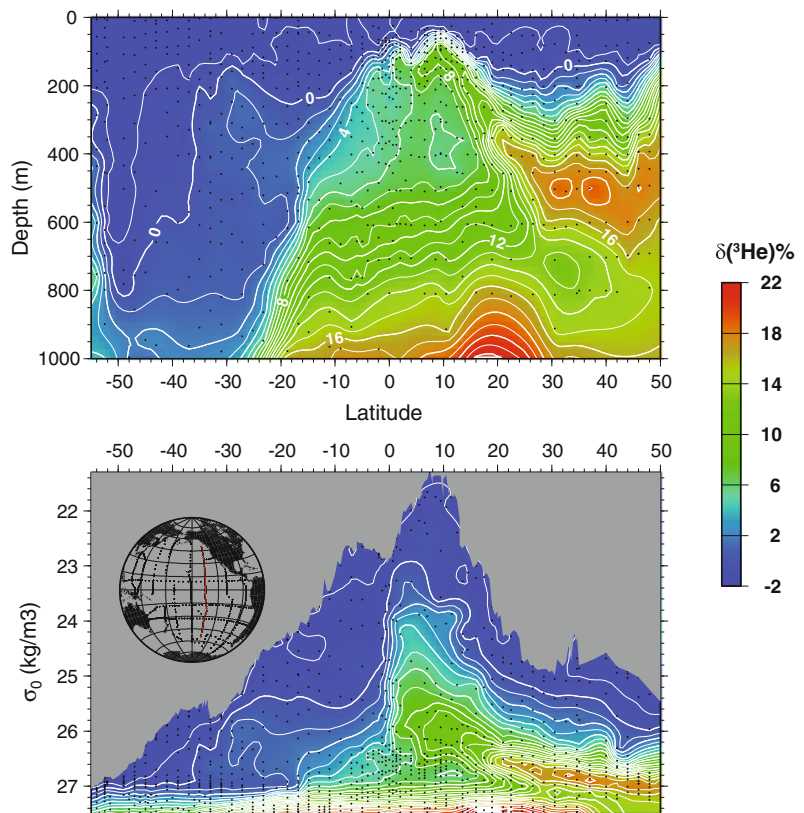
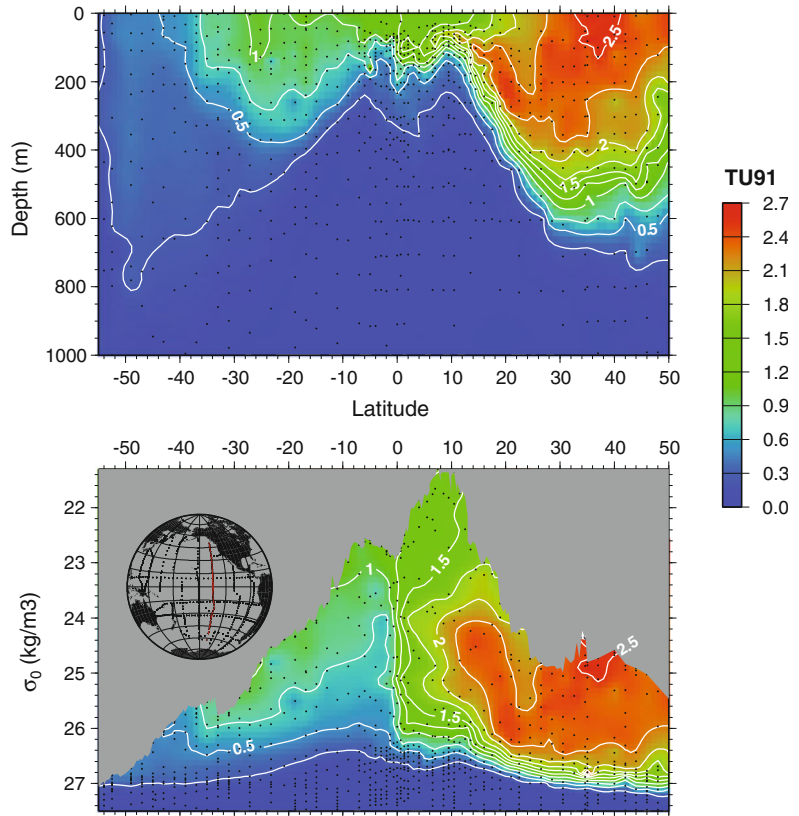


Fig. 8 The distribution of bomb tritium (in $\text{TU}_{91} = 10^{18} \times {}^3\text{H}/{}^1\text{H}$, decay corrected to January 1, 1991) plotted as a function of latitude and depth in meters (*upper panel*) and potential density anomaly in kg m^{-3} (*lower panel*) along WOCE line P17(135°W) in 1991. Positive latitude is north, negative is south. The contour (*white lines*) interval is 0.25 TU_{91} and measurement precision (1 sigma) is 0.005 TU_{91} . The *grey area* in *top part* of the *lower panel* corresponds to density anomalies lighter than the shallowest waters for the corresponding locations. Station locations are indicated as a *red line* in the insert map



approximately $3 \times 10^4 \text{ atoms m}^{-2} \text{ s}^{-1}$. We can compare this to a basin-wide tritium deposition of $\sim 900 \text{ MCi}$ by 1972 (Weiss and Roether 1980), leading to tritiogenic ${}^3\text{He}$ production rate of $1.5 \times 10^5 \text{ atoms m}^{-2} \text{ s}^{-1}$, or about 5 times larger than the volcanic ${}^3\text{He}$ flux.

Mixing further complicates the tritium- ${}^3\text{He}$ age. This can be seen by considering the time-dependent advection–diffusion equation for the age-tracer:

$$\frac{\partial \tau}{\partial t} = \nabla(\kappa \nabla \tau) - \vec{u} \cdot \nabla \tau + 1 + \kappa \left(\frac{\nabla \vartheta}{\vartheta} + \frac{\nabla \zeta}{\zeta} \right) \cdot \nabla \tau$$

[see Jenkins (1987) for a derivation] where κ is the turbulent diffusivity tensor (largely aligned along isopycnal surfaces), ϑ is the tritium concentration and ζ is the sum of tritium and ${}^3\text{He}$ concentrations. The equation closely resembles that of an *ideal age tracer* (one that is advected and diffused) except for the last composite

“non-linear” term, largely driven by the fact that tritium (and hence tritiogenic ${}^3\text{He}$) is a transient tracer. The form of this last term and the typical signs of the ϑ and ζ gradients leads to an augmented “pseudo-velocity” that tends to lower the tritium- ${}^3\text{He}$ age relative to that of an ideal ventilation age (Jenkins 1987).

In directly subtended shallow water regimes such as the shallow thermocline in the eastern subtropical gyres, the non-linear contribution to the age is relatively small (Jenkins 1998; Robbins and Jenkins 1998). However, it can be quite significant for indirectly ventilated regions and deeper in the thermocline (Jenkins 1991, 1998). Using an appropriately designed experiment, *i.e.*, by documenting the three dimensional distribution of these (and other) properties, these terms can be adequately evaluated and robust results can be gained (Jenkins 1998). Moreover, they can be crudely accounted for using box models (Jenkins 1980) or transit time distribution models

(Stanley et al. 2012). Estimates of τ can then be combined with oxygen distributions to calculate oxygen utilization rates, a measure of export production (see Sect. 8.3).

The distributions of ^3He and ^3H in the upper thermocline have been used to investigate thermocline ventilation and shallow ocean circulation in the Northern hemisphere (Jenkins 1998, 2008; Robbins et al. 2000). Jenkins (1998) used a 13 year time-series of ^3H and ^3He in the Sargasso sea, in combination with measurements of salinity and oxygen, to calculate absolute velocities (given by the ^3H and ^3He data combined with geostrophy), isopycnal diffusivities, and oxygen consumption rates. The dilution of the inventory of tritium in the thermocline suggested that the gyre could be considered to have two regions: a western one with cross streamline mixing and an eastern one that is principally advectively ventilated. ^3He and ^3H have also been used to study the ventilation of the lower subtropical thermocline, showing that the Azores current forms a barrier for the southward invasion of mass from isopycnal surface outcrops with only diffusive ventilation across the front for lower thermocline waters (Robbins et al. 2000). More recently, in the East/Japan sea, a time-series of ^3He , ^3H , and CFC data, used in conjunction with a multi-box model, were used to estimate time-changing water mass formation rates and vertical exchange (Jenkins 2008). Jenkins found that there was an approximate order of magnitude decrease in deep water formation rates since the 1960s, accompanied by a shift from sea ice/brine rejection processes to shallow, open ocean convection as the dominant mode of deep and bottom water ventilation.

7 Ocean-Lithosphere Interactions

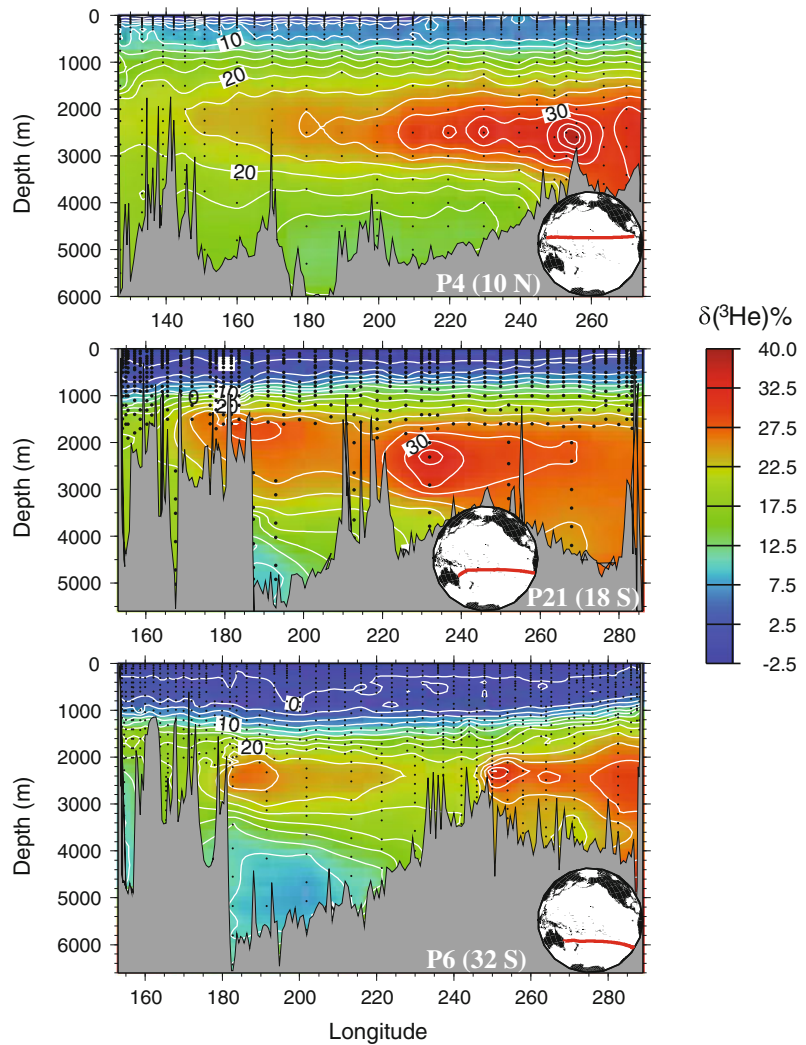
It has been known for more than a century that the residence time of helium in the atmosphere against loss to outer space is of the order of a few million years or less (Bryan 1901; Cook 1902; Stoney 1905)—much shorter than the age of the

earth—and it was supposed that the present day atmospheric inventory of the more abundant isotope ^4He was supported by the degassing of radiogenically produced ^4He from the decay of U and Th series isotopes in the solid earth (Turekian 1959). The residence time of the rarer isotope ^3He in the atmosphere is even shorter (Axford 1968)—less than a million years—and there was a mystery as to how even its meager atmospheric inventory was supported. Production from the decay of cosmic ray produced tritium (Craig and Lal 1961) is at least an order of magnitude too small, as is the lithogenic production by $^6\text{Li}(n, \alpha)^3\text{H} \rightarrow ^3\text{He}$ reactions (Andrews 1985). The neutrons for the latter are produced by thermalization of fast neutrons induced by (α, n) reactions in rocks, where the α particles are produced by decay of U and Th series radionuclides.

The discovery of excess ^3He in Pacific deep waters (Clarke et al. 1969) led to the realization that this isotope was primordial (inherited during the formation of the earth) and emanating from volcanic activity on the seafloor. This conclusion was briefly contested (Fairhall 1970) but shown to be quantitatively sound (Craig and Clarke 1970). The hypothesis was further borne out by subsequent observations near hydrothermal vents (Jenkins et al. 1978, 1980; Lupton et al. 1980; Sakai et al. 1987) and in basaltic glasses from the sea floor (Kurz and Jenkins 1981; Kurz et al. 1983; Lupton and Craig 1975). It also led to the first firm quantification of the present day degassing rate for the earth. Based on radiocarbon chronometry of abyssal waters, the global ^3He degassing rate was estimated to be of the order of 500–1,000 mol y^{-1} (Craig and Clarke 1970) a rate later refined by more sophisticated modeling (Bianchi et al. 2010; Dutay et al. 2004; Farley et al. 1995).

The injection of primordial ^3He into the deep waters occurs at mid-ocean ridges, i.e. sites of active mantle upwelling, and at mantle plume hot spots (e.g. Hawaii and Iceland). The injection of buoyant, very hot ($\sim 350^\circ\text{C}$) water drives vertical plumes which extend hundreds of meters in the water column and are characterized by massive entrainment of surrounding

Fig. 9 Zonal distributions of excess ^3He (largely geophysical) at three latitudes in the Pacific Ocean measured during the WOCE expeditions. The values presented are the dissolved helium $^3\text{He}/^4\text{He}$ isotope ratio anomaly in percent relative to the atmospheric ratio



waters (McDougall 1990; Speer and Rona 1989). Such activity results in clearly discernible horizontal plumes of ^3He that extend from hundreds to even tens of thousands of kilometers (see Fig. 9), tracing deep circulation on basin and global scales. The observation by Lupton and Craig (1981) of a westward emanating ^3He plume at $\sim 15^\circ\text{S}$ in the Pacific apparently running counter to the presumed cyclonic abyssal flow (Stommel and Aarons 1960) prompted Stommel (1982) to point out that these deep plumes are actively driven by the injection of buoyant water at depth, thus influencing the large scale abyssal circulation (Speer 1989).

Substantial excesses of this isotope were observed at active hydrothermal sites (e.g. Jenkins et al. 1978). As a stable conservative tracer, excess ^3He anomalies are visible for tens of thousands of kilometers (Fig. 9). Combining the observed correlation of ^3He and heat in active submarine systems with the known global ^3He flux permits estimates of global convective hydrothermal heat fluxes (Jenkins et al. 1978) although such estimates are limited by local decoupling of the two properties and variations over space and time (Lupton et al. 1989). Nonetheless, use of the ^3He flux gauge for estimating the hydrothermal input of Fe into the

abyssal Pacific provides useful constraints (Boyle and Jenkins 2008) and can be used to estimate global hydrothermal Fe fluxes (Tagliabue et al. 2010).

Because of its persistence in subsurface waters, ^3He excesses can be widely distributed in the ocean, far from its sources. For example, ^3He injected into deep waters in the Pacific can be traced into the Antarctic Circumpolar Current (Garabato et al. 2007; Well et al. 2003) and into the Atlantic Ocean (Jenkins and Clarke 1976; Ruth et al. 2000), where slow seafloor spreading rates result in more modest volcanic ^3He injections. Ruth et al. (2000) have used optimum multiparameter analysis (Tomczak 1981) to separate a local hydrothermal plume signature in the South Atlantic from background contributions from waters of Pacific origin.

Finally, it should be recognized that isotopic ratio of “terrigenic” helium shows substantial variations due to significant variations in the “mantle” helium isotope ratio (Kurz et al. 1982; Kurz et al. 1983), as well as the contribution of radiogenic ^4He due to α -decay of U and Th series isotopes and lithogenic helium due to $^6\text{Li}(n, \alpha)^3\text{H} \rightarrow ^3\text{He}$ reactions (Andrews 1985; Morrison and Pine 1955). It should be possible in principle to evaluate the two contributions by using the saturation anomaly of He in seawater, but the latter is complicated by a variable atmospheric excess driven by surface bubble injection processes (see earlier sections). A variety of schemes have been suggested and used, pioneered first by Bieri and others (Bieri et al. 1964, 1966, 1967; Roether et al. 1998; Well et al. 2001).

8 Biogeochemical Processes

The noble gases, being biologically and chemically inert, cannot give direct information, by themselves, about biological processes in the ocean. However, they can be very useful if combined with biologically active species since the noble gases can constrain physical processes, allowing the biological and physical components to be separated when considering the behavior of the biologically active gas. Gases are useful

tracers of biological production for several reasons. First, the measurements are made in situ, requiring no manipulation of the biological communities, and thus avoiding so called bottle effects (Harrison and Harris 1986; Peterson 1980; Scarratt et al. 2006) that radiotracer bottle incubations may include. Second, the gas tracer based estimates integrate over larger temporal and spatial scales than bottle incubations. For the O_2/Ar pair (Sect. 8.1), the time scale is approximately one to two weeks, depending on the depth of the mixed layer and the magnitude of the gas transfer velocity. For the helium flux gauge technique (Sect. 8.2), the integration occurs over the temporal scale of months to a year and the spatial scale reflects the gyre. For the $^3\text{H}/^3\text{He}$ derived apparent oxygen utilization rates (Sect. 8.3), the temporal scale is several years and the spatial scale reflects the gyre to basin. These long temporal and spatial scales allows the gas tracers to give an integrated view of production, rather than a “snapshot” as may be given by radiotracer bottle incubations, and makes them more likely to catch episodic events such as production stimulated by eddies (McGillicuddy et al. 2007) or storms (Lomas et al. 2009). The different gas tracer systems quantify net community production, new production, and export production, all of which should be equal over long temporal and spatial scales (Eppley and Peterson 1979).

8.1 Oxygen and Argon for Net Community Production

Most of the research in the area of using noble gases to quantify biological production has centered around O_2 and Ar. O_2 is produced by photosynthesis and consumed by respiration, making it reflective of net community production. However, O_2 also responds to physical processes such as thermal warming, gas exchange, and mixing. Ar has similar physicochemical properties to O_2 (Fig. 1), namely nearly identical molecular diffusivity in water and $\sim 10\%$ difference in solubility. These similarities make Ar an ideal abiotic analogue for O_2 . In particular, Ar serves as a good analogue for effects due to warming/cooling and to

bubble injection. However, Ar is not a good analogue for vertical fluxes across the mixed layer, since Ar and O₂ are decoupled below the mixed layer and especially below the euphotic zone, with O₂ decreasing much faster due to remineralization of organic matter. If the O₂ and Ar measurements are interpreted in the framework of a physical model, such as a one-dimensional mixed layer model, the vertical fluxes can be accounted for (Hamme and Emerson 2006; Howard et al. 2010; Spitzer and Jenkins 1989). Including other noble gases, such as He, Ne, Kr and Xe in the model can lead to improved constraints on net community production estimates from the O₂/Ar mass balance (Stanley 2007). However, if only mixed layer measurements of O₂ and Ar are made, then assumptions need to be invoked of steady state production, stable mixed layer depths, and negligible transport of O₂ across base of mixed layer. In regions with a lot of vertical mixing/local upwelling such as in large areas of the Southern Ocean, these assumptions, particularly the latter one, fail; a recent modeling study shows that measurements of O₂/Ar made in mixed layer only and without any corrections for O₂ fluxes tends to underestimate net community production by 5–35 % (Jonsson et al).

The utility of the O₂/Ar pair was first recognized in the late 1980s (Craig and Hayward 1987; Spitzer and Jenkins 1989). These studies estimated net community production rates from either profiles of O₂ and Ar made at discrete locations in the Pacific (Craig and Hayward 1987; Emerson et al. 1991) or from seasonal cycles of oxygen and argon made at a single location in the subtropical North Atlantic (Spitzer and Jenkins 1989). Throughout the next two decades, O₂ and Ar were used to calculate net community production rates throughout the world's oceans, including in the Southern Ocean (Cassar et al. 2007; Hendricks et al. 2004; Reuer et al. 2007), Equatorial Pacific (Hendricks et al. 2005; Stanley et al. 2010), subtropical Pacific (Juraneck and Quay 2005; Quay et al. 2010), and North Pacific (Howard et al. 2010).

A recent exciting advance is the development of small mass spectrometers that can be taken to

sea to measure O₂/Ar continuously in the underway water of a research vessel (Cassar et al. 2009; Kaiser et al. 2005; Tortell 2005). Either a membrane inlet system (Kaiser et al. 2005; Tortell 2005) (in the case of a Membrane Inlet Mass Spectrometer or MIMS) or an equilibrator contact cartridge (in the case of an Equilibrator Inlet Mass Spectrometer or EIMS) (Cassar et al. 2009; Hamme et al. 2012; Stanley et al. 2010) are used in conjunction with a quadrupole mass spectrometer to produce records of net community production with sub-mesoscale resolution. The unprecedented resolution of these NCP records reveals previously unseen variability in NCP, with NCP changing by an order of magnitude on scales as small as tens of kilometers (Fig. 10) (Stanley et al. 2010). Furthermore, in the Western Equatorial Pacific, there is a significant but weak correlation of NCP with temperature and salinity ($R^2 = 0.18$ and 0.33 respectively) with some regions being more strongly correlated and some regions being anticorrelated (Stanley et al. 2010). It is likely that the variations in NCP are related to sub-mesoscale physical processes such as convergence and divergence zones although such a link has not been shown definitively.

8.2 The Helium Flux Gauge for New Production

New production can be estimated from the upward flux of ³He in an approach dubbed the “Helium Flux Gauge” (Jenkins 1988a; Jenkins and Doney 2003). As described in Sect. 6, ³He is the daughter of ³H. Excess ³He is correlated with nitrate in the thermocline because as water ages, it gains in nitrate due to continuing remineralization and gains in ³He due to decay of ³H. When this water is mixed into the euphotic zone, it supplies the nutrients needed for new production and also carries an excess ³He signal. Measurements of ³He in the mixed layer can be combined with a gas exchange relationship to calculate the air-sea flux of excess ³He to the atmosphere. It is imperative that the gas exchange relationship explicitly includes bubbles, since the bubble flux can be a large

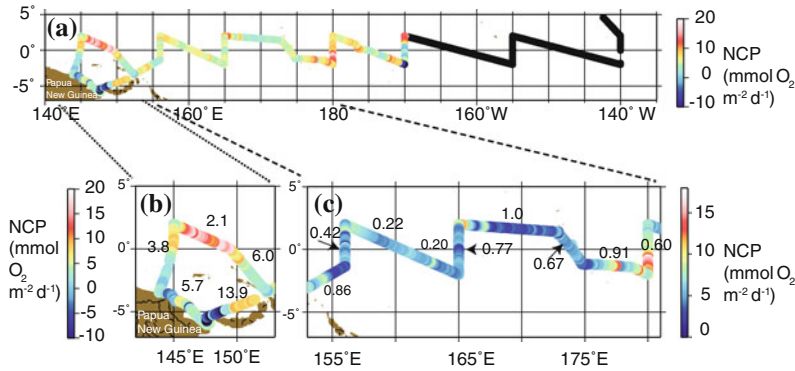


Fig. 10 a Net Community Production (NCP) rates through the equatorial Pacific, as determined by O_2/Ar ratios from an equilibrator inlet mass spectrometer. Negative and “blacked-out” values in the central equatorial Pacific reflect upwelling rather than net heterotrophy. The same data are plotted (b) in larger format for the region

near Papua New Guinea and (c) in larger format with a different color scale for the Western Equatorial Pacific. The numbers reflect the variance-to-mean ratio of NCP along sections of the cruise track. The high-resolution records of O_2/Ar show an enormous amount of small scale variability in NCP. Figure modified from Stanley et al. (2010)

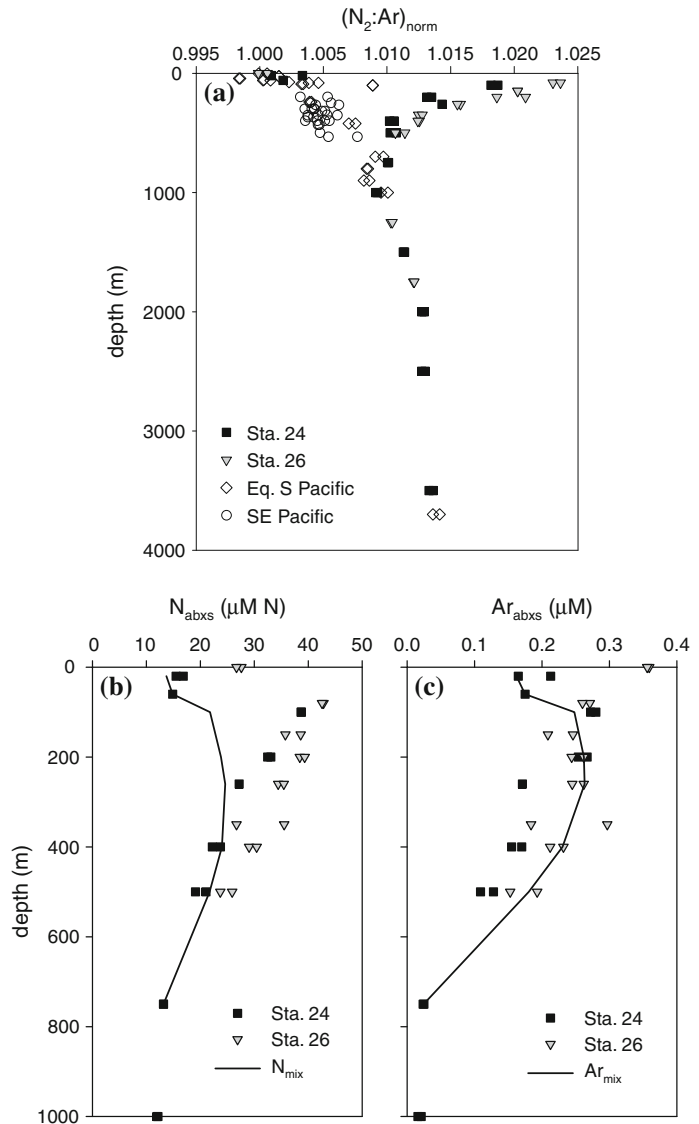
component of the helium flux. This excess 3He flux out of the mixed layer must be balanced by a supply of excess 3He from below on annual or longer time-scales and thus gives a measure of the amount of excess 3He being input to the mixed layer. The correlation between excess 3He and nitrate can then be used to calculate the input of nitrate. Thus this calculation predicts new production based on the physically mediated nitrate flux from vertical transport of thermocline waters—it does not take into account nitrate from other sources such as nitrogen fixation, zooplankton migration (Steinberg et al. 2000) or lateral transport of DON (Mahaffey et al. 2004; Williams and Follows 1998).

This method was first used by Jenkins (1988a) to calculate the rate of new production in the Sargasso Sea from a two year time-series of 3He data. Jenkins and Doney (2003) extended the analysis to a six year time-series of 3He data and found that the nutrient flux, though quantitatively consistent with other observations of production rates, cannot be supplied by local processes. Thus they proposed a three dimensional circulation path by which nutrients are returned to the seasonally accessible surface ocean after being remineralized in the thermocline.

8.3 Oxygen Utilization Rates for Export Production

A third way in which noble gases can be used to quantify biological production is through the use of 3He and 3H to calculate oxygen utilization rates. As described in Sect. 6, 3He and 3H can be combined to calculate τ , the mean age of a water parcel, i.e. the time since the water parcel was subducted. The age of the water can be combined with oxygen data to calculate oxygen utilization rates. If enough 3H and 3He data are collected, then true oxygen utilization rates (OUR) can be calculated (Jenkins 1988b). But if 3H and 3He data are only available at limited locations/times, as is more common, then apparent oxygen utilization rates (AOUR) are calculated, with assumptions being made regarding the path of the water and the initial saturation state of oxygen (Jenkins 1980, 2008; Klein et al. 2003; Stanley et al. 2012; Takahata et al. 2008). The vertically integrated AOUR is a measure of the regional export production; it reflects a projection of geographic and horizontally distributed processes working on individual isopycnal layers (Stanley et al. 2012) rather than local export production.

Fig. 11 **a** Profiles of the ratio of the normalized ratio of N_2/Ar , i.e. $(N_2:Ar)_{norm}$, throughout the SE Pacific including at two stations (Sta 24 and 26) in the Eastern Tropical South Pacific oxygen deficient zone. N_2 , compared to Ar, in oxygen deficient zones is used to calculate denitrification rates. **b** and **c** Depth profiles of observed absolute excess of N_2 and Ar respectively (symbols). The *solid line* denotes the calculated excess due to mixing. Using absolute N_2 and Ar concentrations and a mixing model is an alternative approach for calculating denitrification rates. Figure reproduced from Chang et al. (2010)



8.4 Water Column Denitrification Rates

A fourth application of noble gases to biological processes is the use of N_2/Ar ratios to quantify water column denitrification. Denitrification, i.e. the loss of fixed nitrogen from the ocean, is a key term in the global nitrogen budget but is currently not well constrained, leading to some studies suggesting the nitrogen budget is balanced whereas other studies suggest the budget has a net loss of nitrogen (e.g. Codispoti 2007; Gruber and

Sarmiento 1997). Argon can be paired with N_2 to quantify water column denitrification rates (Chang et al. 2010; Devol et al. 2006; Fuchsman et al. 2008; Manning et al. 2010). The basis behind this technique is that all denitrification processes, whether they stem from NO_3 or NH_3 , will lead to an increase in N_2 . Ar is used to normalize the observed N_2 excesses for physical processes, such as the supersaturation due to mixing (see Sect. 4) and to some extent thermal heating/cooling. The advantages of this technique are that it makes no assumption about the form of

fixed nitrogen consumed, does not rely on the perhaps erroneous assumption of Redfield stoichiometry, and integrates over larger scales than bottle incubations.

Argon has been used in conjunction with N_2 in calculating denitrification rates in two ways. In one method, the N_2/Ar ratio is used (Fig. 11a) (Chang et al. 2010; Devol et al. 2006; Fuchsman et al. 2008; Manning et al. 2010). Profiles of N_2/Ar , normalized to equilibrium values, from oxygen deficient zones (ODZ) show a significant excess of N_2/Ar in the denitrification zone, i.e. region of low O_2 , compared to N_2/Ar profiles from other regions of the ocean (i.e. outside of the ODZ). The N_2/Ar excess can be used to calculate the amount of N_2 lost by denitrification processes. This N_2 loss can then be used in conjunction with an estimate of the residence time of water to calculate the denitrification rate.

In the second method (Chang et al. 2010; Fuchsman et al. 2008), absolute N_2 and Ar concentrations are measured by isotope dilution with a spike of ^{36}Ar (Fig. 11b and c). A two-end member mixing model is used to estimate the effects of diapycnal mixing on the N_2 and Ar concentrations. The absolute N_2 excess can then be calculated by the difference in concentration of N_2 from that predicted by the mixing model. Again, estimates of the residence time of the water are needed to convert the excess N_2 loss into a rate of denitrification.

In the Arabian sea, the N_2/Ar method for calculating denitrification rates gave a rate that was twice as high as that predicted by the more typical “Nitrate-deficit” method—a method that relies on the difference between observed nitrate concentration and Redfield N:P ratios (Devol et al. 2006). The difference is likely to result from one of four causes: (1) non Redfieldian stoichiometry of remineralized matter, perhaps due to nitrogen fixers, leading to errors in the nitrate-deficit method; (2) denitrification of NH_3 which is missed by the nitrate deficit method but included in the N_2/Ar method; (3) water column processes between Fe, Mn, I and N leading to production of N_2 ; (4) sedimentary processes that release N_2 into the overlying water. In the Eastern Tropical South Pacific ODZ, the N_2/Ar method yielded estimates

of denitrification that were only 15–30 % larger than those calculated using the nitrate deficit method (Chang et al. 2010).

9 Summary

Noble gases in seawater, whether measured individually (i.e. 3He for circulation or Ar for diapycnal mixing), as a suite (i.e. measurements of He, Ne, Ar, Kr, and Xe made concurrently for air-sea gas exchange) or in conjunction with biologically active gases (such as O_2/Ar and N_2/Ar), are useful tracers of physical and biological processes. A number of applications of noble gases exist presently and it is likely that more applications will be developed. Until recently, the heavier noble gases (Kr and Xe) were not easily measured. Including Kr and Xe in many of the studies mentioned above could improve the information gleaned from the noble gas distributions.

References

- Andrews JN (1985) The isotopic composition of radiogenic helium and its use to study groundwater movement in confined aquifers. *Chem Geol* 49:339–351
- Axford WI (1968) The polar wind and the terrestrial helium budget. *J Geophys Res* 73:6855–6859
- Benson BB, Krause D Jr (1980) Isotopic fractionation of helium during solution: a probe for the liquid state. *J Solution Chem* 9:895–909
- Beyerle U, Aeschbach-Hertig W, Imboden DM, Baur H, Graf T, Kipfer R (2000) A mass spectrometric system for the analysis of noble gases and tritium from water samples. *Environ Sci Technol* 34(10):2042–2050
- Bianchi D, Sarmiento JL, Gnanadesikan A, Key RM, Schlosser P, Newton R (2010) Low helium flux from the mantle inferred from simulations of oceanic helium isotope data. *Earth Planet Sci Lett* 297:379–386
- Bieri RH, Koide M, Goldberg ED (1964) Noble gases in seawater. *Science* 146(3647):1035–1037
- Bieri RH, Koide M, Goldberg ED (1966) The noble gas contents of Pacific seawaters. *J Geophysical Research* 71:5243–5265
- Bieri RH, Koide M, Goldberg ED (1967) Geophysical implications of excess helium found in Pacific waters. *J Geophys Res* 72(10):2497–2511
- Boyle E, Jenkins W (2008) Hydrothermal iron in the deep western South Pacific. *Geochim Cosmochim Acta* 72(12):A107–A107

- Bryan GH (1901) The kinetic theory of planetary atmospheres. *Philos Trans R Soc (London)* 196(1):1–24
- Cassar N, Barnett BA, Bender ML, Kaiser J, Hamme RC, Tilbrook B (2009) Continuous high-frequency dissolved O-2/Ar measurements by equilibrator inlet mass spectrometry. *Anal Chem* 81(5):1855–1864
- Cassar N, Bender ML, Barnett BA, Fan S, Moxim WJ, Levy H, Tilbrook B (2007) The Southern Ocean biological response to Aeolian iron deposition. *Science* 317(5841):1067–1070
- Chang BX, Devol AH, Emerson S (2010) Denitrification and the nitrogen gas excess in the eastern tropical South Pacific oxygen deficient zone. *Deep-Sea Res Part I-Oceanogr Res Pap* 57(9):1092–1101. doi: [10.1016/j.dsr.2010.05.009](https://doi.org/10.1016/j.dsr.2010.05.009)
- Clarke WB, Beg MA, Craig H (1969) Excess ^3He in the sea: evidence for terrestrial primordial helium. *Earth Planet Sci Lett* 6:213–220
- Codispoti LA (2007) An oceanic fixed nitrogen sink exceeding 400 Tg Na(-1) vs the concept of homeostasis in the fixed-nitrogen inventory. *Biogeosciences* 4(2):233–253
- Cook SR (1902) The permanency of planetary atmospheres, according to the kinetic theory of gases. *Mon Weather Rev* 52(2):401–407
- Craig H, Clarke WB (1970) Oceanic ^3He : contribution from cosmogenic tritium. *Earth Planet Sci Lett* 9: 45–48
- Craig H, Hayward T (1987) Oxygen supersaturation in the ocean: biological versus physical contributions. *Science* 235:199–202
- Craig H, Lal D (1961) The production rate of natural tritium. *Tellus* 13:85–105
- Devol AH, Uhlenhopp AG, Naqvi SWA, Brandes JA, Jayakumar DA, Naik H, Gaurin S, Codispoti LA, Yoshinari T (2006) Denitrification rates and excess nitrogen gas concentrations in the Arabian Sea oxygen deficient zone. *Deep-Sea Res Part I-Oceanogr Res Pap* 53(9):1533–1547. doi: [10.1016/j.dsr.2006.07.005](https://doi.org/10.1016/j.dsr.2006.07.005)
- Doney SC, Glover DM, Jenkins WJ (1992) A model function of the global bomb-tritium distribution in precipitation, 1960–1986. *J Geophys Res* 97:5481–5492
- Doney SC, Jenkins WJ, Bullister JL (1997) A comparison of ocean tracer dating techniques on a meridional section in the eastern North Atlantic. *Deep-Sea Res I* 44(4):603–626
- Dutay J-C, Jean-Baptiste P, Campin J-M, Ishida A, Maier-Reimer E, Matear RJ, Mouchet A, Totterdell IJ, Yamanaka Y, Rodgers KB, Madec G, Orr JC (2004) Evaluation of OCMIP-2 ocean models' deep circulation with mantle helium-3. *J Mar Syst* 48:15–36
- Emerson S, Quay P, Stump C, Wilbur D, Knox M (1991) O₂, Ar, N₂, and ^{222}Rn in surface waters of the subarctic ocean: net biological O₂ production. *Global Biogeochem Cycles* 5:49–69
- Emerson S, Stump C, Wilbur D, Quay P (1999) Accurate measurement of O-2, N-2, and Ar gases in water and the solubility of N-2. *Mar Chem* 64(4):337–347
- Eppley RW, Peterson BJ (1979) Particulate organic matter flux and planktonic new production in the deep ocean. *Nature* 282(677–680):
- Fairhall AW (1970) Concerning the source of the excess ^3He in the sea. *Earth Planet Sci Lett* 7(3):249–250
- Farley KA, Maier-Reimer E, Schlosser P, Broecker WS (1995) Constraints on mantle ^3He fluxes and deep-sea circulation from a general circulation model. *J Geophys Res* 100(B3):3829–3839
- Fuchs G, Roether W, Schlosser P (1987) Excess ^3He in the ocean surface layer. *J Geophys Res* 92:6559–6568
- Fuchsman CA, Murray JW, Konovalov SK (2008) Concentration and natural stable isotope profiles of nitrogen species in the Black Sea. *Mar Chem* 111(1–2): 90–105. doi: [10.1016/j.marchem.2008.04.009](https://doi.org/10.1016/j.marchem.2008.04.009)
- Garabato ACN, Stevens DP, Watson AJ, Roether W (2007) Short-circuiting of the overturning circulation in the Antarctic circumpolar current. *Nature* 447:194–197
- Gehrie E, Archer D, Emerson S, Stump C, Henning C (2006) Subsurface ocean argon disequilibrium reveals the equatorial Pacific shadow zone. *Geophys Res Lett* 33(18):
- Gow AJ, Williamson T (1975) Gas inclusions in antarctic ice sheet and their glaciological significance. *J Geophys Res Oceans Atmos* 80(36):5101–5108. doi: [10.1029/JC080i036p05101](https://doi.org/10.1029/JC080i036p05101)
- Gruber N, Sarmiento JL (1997) Global patterns of marine nitrogen fixation and denitrification. *Global Biogeochem Cycles* 11(2):235–266
- Hamme RC, Cassar N, Lance VP, Vaillancourt RD, Bender ML, Strutton PG, Moore TS, DeGrandpre MD, Sabine CL, Ho DT, Hargreaves BR (2012) Dissolved O₂/Ar and other methods reveal rapid changes in productivity during a Lagrangian experiment in the Southern Ocean. *J Geophys Res-Oceans* 117:C00F12 doi: [10.1029/2011JC007046](https://doi.org/10.1029/2011JC007046)
- Hamme RC, Emerson S (2004a) Measurement of dissolved neon by isotope dilution using a quadrupole mass spectrometer. *Mar Chem* 91(1–4):53–64
- Hamme RC, Emerson S (2004b) The solubility of neon, nitrogen and argon in distilled water and seawater. *Deep Sea Res I* 51(11):1517–1528
- Hamme RC, Emerson S (2006) Constraining bubble dynamics and mixing with dissolved gases: implications for productivity measurements by oxygen mass balance. *J Mar Res* 64(1):73–95
- Hamme RC, Severinghaus JP (2007) Trace gas disequilibria during deep-water formation. *Deep-Sea Res Part I-Oceanogr Res Pap* 54(6):939–950
- Harrison WG, Harris LR (1986) Isotope-dilution and its effects on measurements of nitrogen and phosphorus uptake by oceanic microplankton. *Mar Ecol Prog Ser* 27(3):253–261
- Hendricks MB, Bender ML, Barnett BA (2004) Net and gross O-2 production in the Southern Ocean from measurements of biological O-2 saturation and its triple isotope composition. *Deep-Sea Res Part I-Oceanogr Res Pap* 51(11):1541–1561

- Hendricks MB, Bender ML, Barnett BA, Strutton P, Chavez FP (2005) Triple oxygen isotope composition of dissolved O-2 in the equatorial Pacific: a tracer of mixing, production, and respiration. *J Geophys Res-Oceans* 110(C12):doi:[10.1029/2004JC002735](https://doi.org/10.1029/2004JC002735)
- Henning CC, Archer D, Fung I (2006) Argon as a tracer of cross-isopycnal mixing in the thermocline. *J Phys Oceanogr* 36(11):2090–2105
- Ho DT, Law CS, Smith MJ, Schlosser P, Harvey M, Hill P (2006) Measurements of air-sea gas exchange at high wind speeds in the Southern Ocean: implications for global parameterizations. *Geophys Res Lett* 33(16)
- Ho DT, Wanninkhof R, Schlosser P, Ullman DS, Hebert D, Sullivan KF (2011) Toward a universal relationship between wind speed and gas exchange: gas transfer velocities measured with (3)He/SF(6) during the Southern Ocean gas exchange experiment. *J Geophys Res-Oceans* 116 doi:C00f0410.1029/2010jc006854
- Hohmann R, Schlosser P, Jacobs S, Ludin A, Weppernig R (2002) Excess helium and neon in the southeast Pacific: tracers for glacial meltwater. *J Geophys Res-Oceans* 107(C11):doi:[10.1029/2000JC000378](https://doi.org/10.1029/2000JC000378)
- Holland PR, Feltham DL, Jenkins A (2007) Ice shelf water plume flow beneath filchner-ronne ice shelf, Antarctica. *J Geophys Res-Oceans* 112(C5) doi:C0504410.1029/2006jc003915
- Hood EM, Howes BL, Jenkins WJ (1998) Dissolved gas dynamics in perennially ice-covered Lake Fryxell, Antarctica. *Limnol Oceanogr* 43(2):265–272
- Howard E, Emerson S, Bushinsky S, Stump C (2010) The role of net community production in air-sea carbon fluxes at the North Pacific subarctic-subtropical boundary region. *Limnol Oceanogr* 55(6):2585–2596. doi:[10.4319/lo.2010.55.6.2585](https://doi.org/10.4319/lo.2010.55.6.2585)
- Huang RX, Qiu B (1994) Three dimensional structure of the wind-driven circulation in the subtropical North Pacific. *J Phys Oceanogr* 24(7):1608–1622
- Huang RX, Qiu B (1998) The structure of the wind-driven circulation in the subtropical South Pacific Ocean. *J Phys Oceanogr* 28:1173–1186
- Huber C, Beyerle U, Leuenberger M, Schwander J, Kipfer R, Spahni R, Severinghaus JP, Weiler K (2006) Evidence for molecular size dependent gas fractionation in firm air derived from noble gases, oxygen, and nitrogen measurements. *Earth Planet Sci Lett* 243(1–2):61–73
- Ito T, Deutsch C (2006) Understanding the saturation state of argon in the thermocline: the role of air-sea gas exchange and diapycnal mixing. *Global Biogeochem Cycles* 20(3):doi:[10.1029/2005GB002655](https://doi.org/10.1029/2005GB002655)
- Ito T, Deutsch C, Emerson S, Hamme RC (2007) Impact of diapycnal mixing on the saturation state of argon in the subtropical North Pacific. *Geophys Res Lett* 34(9):doi:[10.1029/2006GL029209](https://doi.org/10.1029/2006GL029209)
- Ito T, Hamme RC, Emerson S (2011) Temporal and spatial variability of noble gas tracers in the North Pacific. *J Geophys Res-Oceans* 116 doi:C0803910.1029/2010jc006828
- Jahne B, Heinz G, Dietrich W (1987) Measurement of the diffusion coefficients of sparingly soluble gases in water. *J Geophys Res* 92(C10):10767–10776
- Jenkins WJ (1977) Tritium-helium dating in the Sargasso Sea: a measurement of oxygen utilization rates. *Science* 196(4287):291–292
- Jenkins WJ (1980) Tritium and He-3 in the Sargasso Sea. *J Mar Res* 38(3):533–569
- Jenkins WJ (1987) ³H and ³He in the Beta Triangle: observations of gyre ventilation and oxygen utilization rates. *J Phys Oceanogr* 17:763–783
- Jenkins WJ (1988a) Nitrate flux into the euphotic zone near Bermuda. *Nature* 331(6156):521–523
- Jenkins WJ (1988b) The use of anthropogenic tritium and He-3 to study sub-tropical gyre ventilation and circulation. *Philos Trans R Soc Lond Ser A Math Phys Eng Sci* 325(1583):43–61
- Jenkins WJ (1991) Determination of isopycnal diffusivity in the Sargasso Sea. *J Phys Oceanogr* 21(7):1058–1061
- Jenkins WJ (1996) Tritium and ³He in the WOCE Pacific program. *Int WOCE Newslett* 23:6–8
- Jenkins WJ (1998) Studying subtropical thermocline ventilation and circulation using tritium and He-3. *J Geophys Res-Oceans* 103(C8):15817–15831
- Jenkins WJ (2008) The biogeochemical consequences of changing ventilation in the Japan/East Sea. *Mar Chem* 108(3–4):137–147. doi:[10.1016/j.marchem.2007.11.003](https://doi.org/10.1016/j.marchem.2007.11.003)
- Jenkins WJ, Beg MA, Clarke WB, Wangersky PJ, Craig H (1972) Excess ³He in the Atlantic Ocean. *Earth Planet Sci Lett* 16:122–130
- Jenkins WJ, Clarke WB (1976) The distribution of ³He in the western Atlantic Ocean. *Deep Sea Res* 23:481
- Jenkins WJ, Doney SC (2003) The subtropical nutrient spiral. *Global Biogeochem Cycles* 17(4):1110. doi:[10.1029/2003GB002085](https://doi.org/10.1029/2003GB002085)
- Jenkins WJ, Edmond JM, Corliss JB (1978) Excess ³He and ⁴He in galapagos submarine hydrothermal waters. *Nature* 272:156
- Jenkins WJ, Rona PA, Edmond JM (1980) Excess ³He in the deep-water over the Mid-Atlantic Ridge at 26°N: evidence of hydrothermal activity. *Earth Planet Sci Lett* 50:39–44
- Jonsson BF, Doney SC, Dunne J, Bender M Evaluation of Southern Ocean O₂/Ar based NCP measurements in a model framework. *J Geophys Res-Oceans*
- Juranek LW, Quay PD (2005) In vitro and in situ gross primary and net community production in the North Pacific subtropical gyre using labeled and natural abundance isotopes of dissolved O-2. *Global Biogeochem Cycles* 19(3):doi:[10.1029/2004GB002384](https://doi.org/10.1029/2004GB002384)
- Kaiser J, Reuer MK, Barnett B, Bender ML (2005) Marine productivity estimates from continuous O-2/Ar ratio measurements by membrane inlet mass spectrometry. *Geophys Res Lett* 32(19):doi:[10.1029/2005GL023459](https://doi.org/10.1029/2005GL023459)
- Klein B, Roether W, Kress N, Manca BB, d'Alcalá MR, Souvermezoglou E, Theocharis A, Civitarese G, Luchetta A (2003) Accelerated oxygen consumption

- in eastern Mediterranean deep waters following the recent changes in thermohaline circulation. *J Geophys Res-Oceans* 108(C9) doi:8107.10.1029/2002jc001454
- Kurz MD, Jenkins WJ (1981) The distribution of helium in oceanic basalt glasses. *Earth Planet Sci Lett* 53:41–54
- Kurz MD, Jenkins WJ, Hart SR (1982) Helium isotopic systematics of oceanic islands and mantle heterogeneity. *Nature* 297(5861):43–47
- Kurz MD, Jenkins WJ, Hart SR, Clague D (1983) Helium isotopic variations in volcanic rocks from Loihi Seamount and the islands of Hawaii. *Earth Planet Sci Lett* 66:388–406
- Lomas MW, Lipschultz F, Nelson DM, Krause JW, Bates NR (2009) Biogeochemical responses to late-winter storms in the Sargasso Sea, I-pulses of primary and new production. *Deep-Sea Res Part I Oceanogr Res Pap* 56(6):843–860
- Loose B, Schlosser P, Smethie WM, Jacobs S (2009) An optimized estimate of glacial melt from the ross ice shelf using noble gases, stable isotopes, and CFC transient tracers. *J Geophys Res-Oceans* 114 doi:C08007.10.1029/2008jc005048
- Lott DE (2001) Improvements in noble gas separation methodology: a nude cryogenic trap. *Geochemistry, Geophysics, Geosystems* 2:10.129/2001GC000202
- Lott DE, Jenkins WJ (1984) An automated cryogenic charcoal trap system for helium isotope mass spectrometry. *Rev Sci Instrum* 55(12):1982–1988
- Lott DE, Jenkins WJ (1998) Advances in analysis and shipboard processing of tritium and helium samples. *Int WOCE Newslett* 30:27–30
- Lupton JE, Baker ET, Massoth GJ (1989) Variable $^3\text{He}/\text{heat}$ ratios in submarine hydrothermal systems: evidence from two plumes over the Juan de Fuca ridge. *Nature* 337:161–164
- Lupton JE, Craig H (1975) Excess He-3 in oceanic basalts: evidence for terrestrial primordial helium. *Earth Planet Sci Lett* 26(2):133–139
- Lupton JE, Craig H (1981) A major helium-3 source at 15S on the East Pacific rise. *Science* 214(4516):13–18
- Lupton JE, Klinkhammer G, Normark WR, Haymon R, MacDonald KC, Weiss RF, Craig H (1980) Helium-3 and manganese at the 21 N East Pacific rise hydrothermal site. *Earth Planet Sci Lett* 50:115–127
- Luyten JR, Pedlosky J, Stommel H (1983) The ventilated thermocline. *J Phys Oceanogr* 13:292–309
- MacMahon D (2006) Half-life evaluations for H-3, Sr-90, and Y-90. *Appl Radiat Isot* 64(10–11):1417–1419
- Mahaffey C, Williams RG, Wolff GA, Anderson WT (2004) Physical supply of nitrogen to phytoplankton in the Atlantic Ocean. *Global Biogeochem Cycles* 18(1):
- Manning CC, Hamme RC, Bourbonnais A (2010) Impact of deep-water renewal events on fixed nitrogen loss from seasonally-anoxic Saanich inlet. *Mar Chem* 122(1–4):1–10. doi:10.1016/j.marchem.2010.08.002
- Martinerie P, Raynaud D, Etheridge DM, Barnola JM, Mazaudier D (1992) Physical and climatic parameters which influence the air content in polar ice. *Earth Planet Sci Lett* 112(1–4):1–13. doi:10.1016/0012-821x(92)90002-d
- McDougall TJ (1990) Bulk properties of “hot smoker” plumes. *Earth Planet Sci Lett* 99:185–194
- McGillicuddy DJ, Anderson LA, Bates NR, Bibby T, Buesseler KO, Carlson CA, Davis CS, Ewart C, Falkowski PG, Goldthwait SA, Hansell DA, Jenkins WJ, Johnson R, Kosnyrev VK, Ledwell JR, Li QP, Siegel DA, Steinberg DK (2007) Eddy/wind interactions stimulate extraordinary mid-ocean plankton blooms. *Science* 316(5827):1021–1026
- Morrison P, Pine J (1955) Radiogenic origin of helium isotopes in rock. *Ann N Y Acad Sci* 62(3):69–92
- Nicholson D, Emerson S, Caillon N, Jouzel J, Hamme RC (2010) Constraining ventilation during deepwater formation using deep ocean measurements of the dissolved gas ratios (40)Ar/(36)Ar, N(2)/Ar, and Kr/Ar. *J Geophys Res Oceans* 115 doi:C11015. 10.1029/2010jc006152
- Nightingale PD, Malin G, Law CS, Watson A, Liss PS, Liddicoat MI, Boutin J, Upstill-Goddard R (2000) In situ evaluation of air-sea gas exchange parameterizations using novel conservative and volatile tracers. *Global Biogeochem Cycles* 14(1):373–387
- Peterson BJ (1980) Aquatic primary productivity and the C-14-Co2 method—a history of the productivity problem. *Annu Rev Ecol Syst* 11:359–385
- Postlethwaite CF (2002) Developing a tool for evaluating the role of seasonal sea ice in deepwater formation. University of Southampton
- Postlethwaite CF, Rohling EJ, Jenkins WJ, Walker CF (2005) A tracer study of ventilation in the Japan/East Sea. *Deep Sea Res Part II* 52(11–13):1684–1704
- Quay PD, Peacock C, Bjorkman K, Karl DM (2010) Measuring primary production rates in the ocean: enigmatic results between incubation and non-incubation methods at station ALOHA. *Global Biogeochem Cycles* 24(3):doi:10.1029/2009GB003665
- Reuer MK, Barnett BA, Bender ML, Falkowski PG, Hendricks MB (2007) New estimates of Southern Ocean biological production rates from O-2/Ar ratios and the triple isotope composition of O-2. *Deep-Sea Res Part I Oceanogr Res Pap* 54(6):951–974
- Robbins PE, Jenkins WJ (1998) Observations of temporal changes of tritium- ^3He age in the eastern North Atlantic thermocline: evidence for changes in ventilation? *J Mar Res* 56:1125–1161
- Robbins PE, Price JF, Owens WB, Jenkins WJ (2000) The importance of lateral diffusion for the ventilation of the lower thermocline in the subtropical North Atlantic. *J Phys Oceanogr* 30(1):67–89. doi: 10.1175/1520-0485(2000)030<0067:tioldf>2.0.co;2
- Rodehacke CB, Hellmer HH, Huhn O, Beckmann A (2007) Ocean/ice shelf interaction in the southern Weddell Sea: results of a regional numerical helium/neon simulation. *Ocean Dyn* 57(1):1–11
- Roether W, Well R, Putzka A, Ruth C (1998) Component separation of oceanic helium. *J Geophys Res* 103(C12):27931–27946
- Runham G (2001) Laboratory determination of the partitioning of He, Ne, and Ar between seawater and ice during freezing. University of Southampton

- Ruth C, Well R, Roether W (2000) Primordial ^3He in South Atlantic deep waters from sources on the Mid-Atlantic ridge. *Deep Sea Res I* 47:1059–1075
- Sakai H, Tsubota H, Nakai T, Ishibashi J, Akagi T, Gamoto T, Tilbrook B, Igarashi G, Kodera M, Shitashima K, Nakamura S, Fujioka K, Watanabe M, McMurtry G, Malahoff A, Ozima M (1987) Hydrothermal activity on the summit of Loihi Seamount. *Geochem J* 21:11–21
- Salter ME, Upstill-Goddard RC, Nightingale PD, Archer SD, Blomquist B, Ho DT, Huebert B, Schlosser P, Yang M (2011) Impact of an artificial surfactant release on air-sea gas fluxes during deep ocean gas exchange experiment II. *J Geophys Res Oceans* 116 doi:C11016 [10.1029/2011jc007023](https://doi.org/10.1029/2011jc007023)
- Sano Y, Takahata N (2005) Measurement of noble gas solubility in seawater using a quadrupole mass spectrometer. *J Oceanogr* 61(3):465–473
- Scarratt MG, Marchetti A, Hale MS, Rivkin RB, Michaud S, Matthews P, Levasseur M, Sherry N, Merzouk A, Li WKW, Kiyosawa H (2006) Assessing microbial responses to iron enrichment in the subarctic Northeast Pacific: do microcosms reproduce the in situ condition? *Deep Sea Res Part II* 53(20–22):2182–2200
- Schlosser P (1986) Helium: a new tracer in Antarctic oceanography. *Nature* 321:233–235
- Schlosser P, Bayer R, Flodvik A, Fammelsrod T, Rhohardt G, Munnich KO (1990) Oxygen 18 and helium as tracers of ice shelf water and water/ice interaction in the Weddell Sea. *J Geophys Res* 95:3253–3263
- Severinghaus JP, Grachev A, Luz B, Caillon N (2003) A method for precise measurement of argon 40/36 and krypton/argon ratios in trapped air in polar ice with applications to past firn thickness and abrupt climate change in Greenland and at Siple Dome, Antarctica. *Geochim Cosmochim Acta* 67(3):325–343
- Smedsrud LH, Jenkins A (2004) Frazil ice formation in an ice shelf water plume. *J Geophys Res Oceans* 109(C3) doi:C03025 [10.1029/2003jc001851](https://doi.org/10.1029/2003jc001851)
- Smith MJ, Ho DT, Law CS, McGregor J, Popinet S, Schlosser P (2011) Uncertainties in gas exchange parameterization during the SAGE dual-tracer experiment. *Deep Sea Res Part II* 58(6):869–881. doi: [10.1016/j.dsr2.2010.10.025](https://doi.org/10.1016/j.dsr2.2010.10.025)
- Smith SP, Kennedy BM (1983) The solubility of noble gases in water and NaCl brine. *Geochim Cosmochim Acta* 47(3):503–515. doi: [10.1016/0016-7037\(83\)90273-9](https://doi.org/10.1016/0016-7037(83)90273-9)
- Speer KG (1989) The Stommel and Arons model and geothermal heating in the South Pacific. *Earth Planet Sci Lett* 95:359–366
- Speer KG, Rona PA (1989) A model of an Atlantic and Pacific hydrothermal plume. *J Geophys Res* 94:6213–6220
- Spitzer WS, Jenkins WJ (1989) Rates of vertical mixing, gas-exchange and new production—estimates from seasonal gas cycles in the upper ocean near Bermuda. *J Mar Res* 47(1):169–196
- Stanley RHR (2007) Air-sea gas exchange and upper ocean biological production. Ph.D thesis, MIT/WHOI Joint Program
- Stanley RHR, Baschek B, Lott DE, Jenkins WJ (2009a) A new automated method for measuring noble gases and their isotopic ratios in water samples. *Geochim Geophys Geosyst* 10:doi:[10.1029/2009GC002429](https://doi.org/10.1029/2009GC002429)
- Stanley RHR, Doney SC, Jenkins WJ, Lott III DE (2012) Apparent oxygen utilization rates calculated from tritium and helium-3 profiles at the Bermuda Atlantic time-series study site. *Biogeosciences* doi:[10.5194/bg-9-1969-2012](https://doi.org/10.5194/bg-9-1969-2012):9977-10015
- Stanley RHR, Jenkins WJ, Doney SC (2006) Quantifying seasonal air-sea gas exchange processes using noble gas time-series: a design experiment. *J Mar Res* 64(2):267–295
- Stanley RHR, Jenkins WJ, Doney SC, Lott III DE (2009b) Noble gas constraints on air-sea gas exchange and bubble fluxes. *J Geophys Res Oceans* 114:doi:[10.1029/2009JC005396](https://doi.org/10.1029/2009JC005396)
- Stanley RHR, Kirkpatrick JB, Barnett B, Cassar N, Bender ML (2010) Net community production and gross production rates in the Western Equatorial Pacific. *Global Biogeochem Cycles* 24:GB4001, doi:40 [10.1029/2009GB003651](https://doi.org/10.1029/2009GB003651)
- Steinberg DK, Carlson CA, Bates NR, Goldthwait SA, Madin LP, Michaels AF (2000) Zooplankton vertical migration and the active transport of dissolved organic and inorganic carbon in the Sargasso Sea. *Deep Sea Res I* 47:137–158
- Stommel H (1982) Is the South Pacific helium-3 plume dynamically active? *Earth Planet Sci Lett* 61:63–67
- Stommel H, Aarons AB (1960) On the abyssal circulation of the world ocean—II. An idealized model of the circulation pattern and amplitude in ocean basins. *Deep Sea Res* 6:217–233
- Stoney GJ (1905) Escape of gases from the atmosphere. *Mon Weather Rev* 7(January):6–9
- Tagliabue A, Bopp L, Dutay J-C, Bowie AR, Chever F, Jean-Baptiste P, Bucciarelli E, Lannuzel D, Remenyi T, Sarthou G, Aumont O, Gehlen M, Jeandel C (2010) Hydrothermal contribution to the oceanic dissolved iron inventory. *Nat Geosci* 3(4):252–256
- Takahashi T, Williams RT et al (1988) Alteration of the concentrations of dissolved gases in Niskin bottles during sampling operations. SAVE technical report
- Takahata N, Sano Y, Horigucut K, ShiraO' K, Ganio T (2008) Helium isotopes of seawater in the Japan Sea. *J Oceanogr* 64(2):293–301. doi: [10.1007/s10872-008-0023-3](https://doi.org/10.1007/s10872-008-0023-3)
- Thorpe SA (1984) A model of the turbulent diffusion of bubbles below the sea surface. *J Phys Oceanogr* 14:841–854
- Tomczak M (1981) A multi-parameter extension of temperature/salinity diagram techniques for the analysis of non-isopycnal mixing. *Prog Oceanogr* 10:147–171
- Tortell PD (2005) Dissolved gas measurements in oceanic waters made by membrane inlet mass spectrometry. *Limnol Oceanogr Methods* 3:24–37
- Turekian KK (1959) The terrestrial economy of helium and argon. *Geochim Cosmochim Acta* 17:37–43
- Warner MJ, Bullister JL, Wisegarver DP, Gammon RH, Weiss RF (1996) Basin-wide distributions of

- chlorofluorocarbons CFC-11 and CFC-12 in the North Pacific: 1985–1989. *J Geophys Res* 101:20525–20542
- Watson AJ, Upstill-Goddard RC, Liss PS (1991) Air-sea gas exchange in rough and stormy seas measured by a dual-tracer technique. *Nature* 349:145–147
- Weiss RF (1968) Piggyback sampler for dissolved gas studies on sealed water samples. *Deep Sea Res* 15: 841–854
- Weiss RF (1970) Helium isotope effect in solution in water and seawater. *Science* 168:247–248
- Weiss RF (1971) Solubility of helium and neon in water and seawater. *J Chem Eng Data* 16:235–241
- Weiss RF, Kyser TK (1978) Solubility of krypton in water and seawater. *J Chem Eng Data* 23(1):69–72
- Weiss WM, Roether W (1980) The rates of tritium input to the world oceans. *Earth Planet Sci Lett* 49:435–446
- Well R, Lupton JE, Roether W (2001) Crustal helium in deep Pacific waters. *J Geophys Res* 106(C7):14165–14177
- Well R, Roether W, Stevens DP (2003) An additional deep-water mass in drake passage as revealed by ^3He data. *Deep Sea Res I* 50(9):1079–1098
- Weppernig R, Schlosser P, Khattiwala S, Fairbanks RG (1996) Isotope data from ice station Weddell: implications for deep water formation in the Weddell sea. *J Geophys Res Oceans* 101(C11):25723–25739. doi:[10.1029/96jc01895](https://doi.org/10.1029/96jc01895)
- Wijffels SE, Toole JM, Bryden HL, Fine RA, Jenkins WJ, Bullister JL (1996) The water masses and circulation at 10°N in the Pacific. *Deep Sea Res I* 43(4):501–544
- Wijffels SE, Toole JM, Davis RE (2001) Revisiting the South Pacific subtropical circulation: a synthesis of WOCE observations along 32 S. *J Geophys Res* 106(C9):19481–19513
- Williams RG, Follows MJ (1998) The Ekman transfer of nutrients and maintenance of new production over the North Atlantic. *Deep Sea Res Part I Oceanogr Res Pap* 45(2–3):461–489
- Wise DL, Houghton G (1966) Diffusion coefficients of 10 slightly soluble gases in water at 10–60°C. *Chem Eng Sci* 21(11):999–1010. doi:[10.1016/0009-2509\(66\)85096-0](https://doi.org/10.1016/0009-2509(66)85096-0)
- Wood D, Caputi R (1966) Solubilities of Kr and Xe in fresh and sea water. In: U.S. Naval Radiological Defense Laboratory, San Francisco, p 14
- Young C, Lupton JE (1983) An ultra tight fluid sampling system using cold-welded copper tubing. *Eos Transactions AGU* 64:735